Section 3 Optics and Devices

Chapter 1. Optics and Quantum Electronics

Academic and Research Staff

Professor Hermann A. Haus, Professor Erich P. Ippen, Professor James G. Fujimoto, Professor Peter L. Hagelstein, Dr. Brett E. Bouma, Dr. Jay N. Damask

Visiting Scientists and Research Affiliates

Dr. Mark E. Brezinski,[1] Dr. Katherine L. Hall, Dr. Jürgen Herrmann,[2] Dr. Stefano Longhi, Dr. Mordehai Margalit, Dr. Masayuki Matsumoto, Dr. Victor P. Mikhailov,[3] Leo J. Missaggia,[4] Dr. Shu Namiki, Dr. Dominique S. Peter, Dr. Carmen Puliafito,[5] Dr. Joel Schuman,[6] Dr. Günter Steinmeyer, Eric A. Swanson,[7] Gaston Tudury, Dr. James N. Walpole[8]

Graduate Students

Igor P. Bilinsky, Stephen A. Boppart, Po-Hsiu Cheng, Seong-Ho Cho, Patrick C. Chou, David J. Dougherty, John M. Fini, Matthew E. Grein, Boris Golubovic, Michael R. Hee, David J. Jones, Farzana I. Khatri, Mohammed J. Khan, Christina Manolatou, Lynn E. Nelson, Costantinos Pitris, Rohit Prasankumar, Daniel J. Ripin, Susan Sujono, Guillermo J. Tearney, Erik R. Thoen, Constantine Tziligakis, William S. Wong, Charles Yu

Undergraduate Students

Ravindra V. Dalal

Technical and Support Staff

Mary C. Aldridge, Donna L. Gale, Cynthia Y. Kopf

1.1 Modelocked Lasers using Erbium-doped Glass Waveguide Amplifiers

Sponsors

Defense Advanced Research Projects Agency
Grant F49620-96-0126
U.S. Air Force - Office of Scientific Research
Grant F49620-98-1-0139

Project Staff

David J. Jones, Professor Hermann A. Haus, Professor Erich P. Ippen, Dr. Shu Namiki

In our past work on short-pulse fiber lasers, we have developed both soliton and stretched-pulse fiber lasers.[9] These fiber lasers, which operate in the 1.5 μm region, have utilized erbium-doped fiber (EDF) as the gain element. Recently, erbium-doped planar waveguide amplifiers have been developed as an alternative to EDF.[10] With a typical length of 4.5 cm these integrated optical amplifiers are able to deliver

1 Research Affiliate, Cardiac Unit, Massachusetts General Hospital and Harvard Medical School, Boston, Massachusetts.

2 MIT Lincoln Laboratory, Lexington, Massachusetts.

3 International Laser Center, Polytechnical Academy, Minsk, Belarus.

4 MIT Lincoln Laboratory, Lexington, Massachusetts.

5 Chairman, Department of Ophthalmology, Tufts University Medical School and Director, New England Eye Center, Boston, Massachusetts.

6 Director, Glaucoma Services, New England Eye Center, Tufts New England Medical Center, Boston, Massachusetts.

7 MIT Lincoln Laboratory, Lexington, Massachusetts.

8 Ibid.

9 L.E. Nelson, D.J. Jones, K. Tamura, H.A. Haus, and E.P. Ippen, "Ultrashort-Pulse Fiber Ring Lasers," *Appl. Phys. B* 65: 277 (1997).

10 D. Barbier, M. Rattay, F. Saint Andre, G. Clauss, M. Trouillon, A. Kevorkian, J.-M. P. Delavaux, and E. Murphy, "Amplifying Four-Wavelength Combiner, Based on Erbium/Ytterbium-Doped Waveguide Amplifiers and Integrated Splitters," *IEEE Photonics Technol. Lett.* 9: 315 (1997).

10 dB of gain at 1.53 μm with 980 nm pump powers of 130 mW. In this project we investigated the operating characteristics and performance of a modelocked soliton fiber laser using such a waveguide amplifier as the gain element.[11]

The key advantage of using waveguide amplifiers in modelocked fiber lasers is a sharp reduction in cavity length, allowing fundamental repetition rates of 100-300 MHz. Another advantage is the possible on-chip fabrication of a wavelength-division-multiplexing pump coupler to create a truly compact integrated optical component for constructing modelocked fiber lasers. But most importantly, a short cavity simultaneously reduces two parasitic effects that limit the performance of soliton fiber lasers[12]: resonant sideband formation and saturation of the polarization additive pulse modelocking (P-APM) mechanism.

Similar to long distance transmission systems, dispersive waves generated by periodic perturbations in the laser cavity form resonant sidebands. In the case of soliton fiber lasers, the pulse width is limited by sideband generation when the soliton period Z_0 approaches the cavity length Z_c. Since Z_0 is proportional to τ^2, this condition effectively clamps the pulse width. By reducing the cavity length to 1.3 m, (while keeping the net dispersion strongly anomalous to maintain a high pulse energy) generation of significantly shorter solitons becomes possible.

An additional effect that limits the peak power (and hence the pulse energy) of soliton fiber lasers is saturation of the P-APM mechanism. This condition occurs because of the interferometric nature of P-APM which has a sinusoidal dependence of transmission with peak power. As a result, most soliton fiber lasers tend to multipulse at high pump powers. Shortening the total fiber length to 1.3 m reduces the net nonlinearity per pass, thus avoiding P-APM saturation and production of multiple pulses.

By incorporating a waveguide amplifier into a fiber laser, the resulting short cavity (1.3 m of fiber) generated 113 fs solitons with a pulse energy of 160 pJ at a fundamental repetition rate of 130 MHz. Presently, work is continuing on shorter cavities in an effort to generate even shorter pulses at fundamental repetition rates greater than 500 MHz.

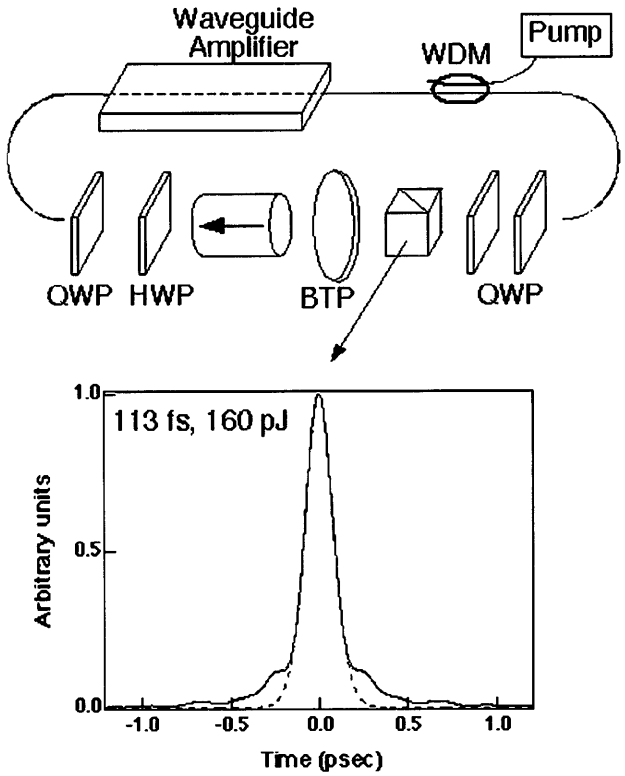

Figure 1. Cavity diagram of modelocked fiber laser using a waveguide amplifier. QWP, quarter-wave plate; HWP, half-wave plate; BTP, birefringent tuning plate; WDM, wavelength-division-multiplexer. Inset is an intensity autocorrelation of output pulse with sech-fit (dashed line). The pulse-width is 113 fs.

1.2 Publications

Barbier, D., M. Rattay, F. Saint Andre, G. Clauss, M. Trouillon, A. Kevorkian, J.-M. P. Delavaux, and E. Murphy. "Amplifying Four-Wavelength Combiner, Based on Erbium/Ytterbium-Doped Waveguide Amplifiers and Integrated Splitters." *IEEE Photonics Technol. Lett.* 9: 315 (1997).

Jones, D.J., S. Namiki, D. Barbier, E.P. Ippen, and H.A. Haus. "116-fs Soliton Source Based on an Er-Yb Co-doped Planar Waveguide Amplifier." *IEEE Photonics Technol. Lett.* Forthcoming.

11 D.J. Jones, S. Namiki, D. Barbier, E.P. Ippen, and H.A. Haus, "116-fs Soliton Source Based on an Er-Yb Co-doped Planar Waveguide Amplifier," *IEEE Photonics Technol. Lett.*, forthcoming; D.J. Jones, S. Namiki, D. Barbier, E.P. Ippen, and H.A. Haus, "Passively Modelocked Fiber Laser using an Er-Yb Co-Doped Planar Waveguide Amplifier," paper presented at Optical Fiber Communications '98, San Jose, California, February 22-28, 1998.

12 L.E. Nelson, D.J. Jones, K. Tamura, H.A. Haus, and E.P. Ippen, "Ultrashort-Pulse Fiber Ring Lasers," *Appl. Phys. B* 65: 277 (1997).

Jones, D.J., S. Namiki, D. Barbier, E.P. Ippen, and H.A. Haus. "Passively Modelocked Fiber Laser using an Er-Yb Co-Doped Planar Waveguide Amplifier." Paper presented at Optical Fiber Communications '98, San Jose California, February 22-28, 1998.

Nelson, L.E., D.J. Jones, K. Tamura, H.A. Haus, and E.P. Ippen. "Ultrashort-Pulse Fiber Ring Lasers." *Appl. Phys. B* 65: 277 (1997).

1.3 Environmentally-Stable Stretched-Pulse Fiber Laser

Sponsors

Defense Advanced Research Projects Agency
Joint Services Electronics Program
U.S. Air Force - Office of Scientific Research

Project Staff

David J. Jones, Lynn E. Nelson, Professor Hermann A. Haus, Professor Erich P. Ippen

Previous versions of our stretched-pulse fiber lasers[13] have been passively modelocked via polarization additive pulse modelocking (P-APM) in a self-starting ring cavity with non-polarization maintaining (PM) fiber. Such a configuration is sensitive to mechanical and temperature variations which may induce drifts in the polarization bias of the P-APM and thus affect its environmental stability. Previously reported environmentally-stable soliton fiber lasers have used a linear topology and a Faraday mirror (FRM) to eliminate linear bias drift. As a step towards obtaining high powers and broader spectra, we have developed an environmentally-stable stretched-pulse fiber laser that uses a sigma cavity design.[14]

The cavity construction is shown in Figure 2. Pulse shaping via P-APM occurs only in the pigtail section and the FRM eliminates any P-APM environmental dependence. Emerging from the P-APM transmission port, a portion of the pulse is tapped off via a variable output coupler which provides a high quality pulse. After filtering, the pulse propagates through the anomalous dispersion ring constructed of PM fiber in a linear polarization state and then is injected back into the P-APM pigtail section. PM fiber in the ring section ensures environmental stability in this portion of the cavity.

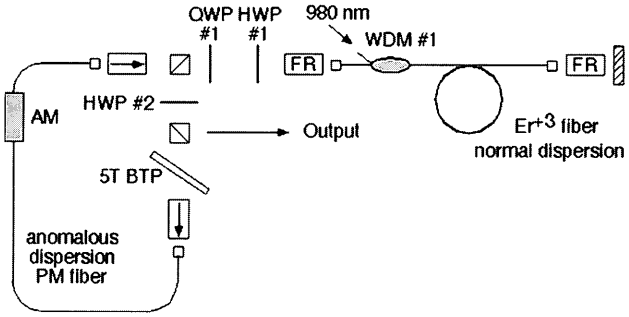

Figure 2. Stretched-pulse sigma cavity. WDM, wave-length division multiplexer; FR, Faraday rotator; BTP, birefringent tuning plate; AM, amplitude modulator; QWP, quarter wave plate; HWP, half wave plate; PM, polarization maintaining.

The sigma design is not a traveling-wave cavity through its entire length. First-order reflections from bulk elements in the linear section of the cavity can form etalons which impede self-starting via mode-pulling.[15] Spatial hole-burning in the erbium-doped fiber is an additional hindrance for self-starting.[16] To overcome these obstacles, a fiber pigtailed $LiNbO_3$ traveling-wave modulator is included in the ring section of the cavity for assistance with pulse start-up. After modelocking is initiated by turning on the modulator and adjusting the wave-plates and filter, the modulator is turned off and single pulse operation remains. By relying on the modulator to provide pulse start-up, a high-energy pulse state can be directly obtained with diode pump levels of < 200 mW. This is a significant aspect of this laser as it represents the first high-power stretched-pulse erbium-doped fiber laser which can be pumped by conventional laser diodes.

13 L.E. Nelson, D.J. Jones, K. Tamura, H.A. Haus, and E.P. Ippen, "Ultrashort-Pulse Fiber Ring Lasers," *Appl. Phys. B* 65: 277 (1997).

14 D.J. Jones, H.A. Haus, L.E. Nelson, and E.P. Ippen, "Stretched Pulse Generation and Propagation," accepted to *IEICE of Japan* special issue on Ultrashort Pulse Technologies and their Applications, forthcoming; D.J. Jones, L. E. Nelson, H.A. Haus, and E.P. Ippen, "Diode-Pumped Environmentally Stable Stretched-Pulse Fiber Laser," *IEEE J. Select. Topics Quantum Electron.* 3: 1076 (1997); D.J. Jones, L. E. Nelson, H.A. Haus, and E.P. Ippen, "Environmentally Stable Stretched Pulse Fiber Laser Generating 120 fs Pulses," paper CTuY3, Conference on Lasers and Electro-Optics '97, Baltimore, Maryland, May 18-23, 1997.

15 K. Tamura, J. Jacobson, E.P. Ippen, H.A. Haus, and J.G. Fujimoto, "Unidirectional Ring Resonators for Self-Starting Passively Mode-Locked Lasers," *Opt. Lett.* 18: 220 (1993).

16 F. Krausz and T. Brabec, "Passive Mode Locking in Standing Wave Laser Resonators," *Opt. Lett.* 18: 888 (1993).

Following the previously described start-up procedure, this laser generates nanojoule pulses with 50 nm of spectral width that are compressible to sub-100 fs. Environmental stability is verified by imposing local temperature changes of +35 degrees Celsius at various points on the fiber with a heat gun. Even under these conditions the sigma laser remained stably modelocked. Mechanical perturbations appropriate to research-grade laser packaging also failed to disrupt modelocking. Overall turn-key operation with the sigma laser was observed over a period of months. Presently we are working with Clark-MXR, Inc. to develop this version of the stretched-pulse laser into a commercial product.

1.4 High-Repetition Rate Laser Sources

Sponsors

Defense Advanced Research Projects Agency
U.S. Air Force - Office of Scientific Research

Project Staff

Matthew E. Grein, Dr. Mordehai Margalit, Professor Erich P. Ippen, Professor Hermann A. Haus

Active modelocking is an attractive technique for applications requiring synchronization of a laser to an external clock. For an ultra-high speed telecommunications system employing time-division-multiplexed (TDM) channels, the requirements for such a laser source include repetition rates in excess of 10 Gbit/s, pulsewidths on the order of one picosecond, and low amplitude and timing jitter.

The pulsewidths expected from a fiber laser with active modelocking alone, at 10 GHz, are on the order of 3-4 picoseconds. This group[17] has previously shown theoretically[18] and experimentally that much shorter pulses can be achieved by taking advantage of soliton formation in the fiber. Graduate student David J. Jones has previously demonstrated 624 fs pulses at 5 GHz, and graduate student Matthew Grein has recently achieved 600 fs pulses at 10 GHz. These pulsewidths are shorter by a factor of 4 than those predicted by the Siegman-Kuizenga theory[19] and appear to be consistent with the theory of Kärtner.[20] These are important results for two reasons: they verify that solitonic effects produce the pulse shortening predicted by theory, and they demonstrate that we can directly generate sub-picosecond pulses at high repetition rates. In fact, 600 fs pulses are the shortest pulses reported to date, directly generated at 10 GHz.

In achieving these recent results, we have shown that filtering plays an extremely important role in the operation of the laser. Indeed, we have found that using the broadest filters leads to the shortest pulses. While that fact may not seem so surprising, we found that, in addition, opening up the filter bandwidth did not come at the expense of pulse-to-pulse amplitude fluctuations. Here again, we find beneficial features of soliton formation: soliton effects with the addition of spectral filtering provide an intensity-dependent loss.[21] The explanation is that shorter pulses have the broadest spectra, thus see the most loss in the filter. The spectral loss discourages the buildup of a single, very short pulse and encourages the equalization of pulse energies among the time slots.

An illustration of the laser output is given in Figure 3. The autocorrelation displays a background-free 1.0 picosecond pulse and rf sidemode suppression greater than 55 dB, indicating that the amplitude fluctuations are less than 0.0003%, or a possible pulse dropout rate of 1 every 316200 pulses.

17 D.J. Jones, H.A. Haus, and E.P. Ippen, "Sub-Picosecond Solitons in an Actively Mode-Locked Fiber Laser," *Opt. Lett.* 2: 1818 (1996); M.E. Grein, *A Regeneratively Modelocked, Fiber Ring Laser,* M.S. thesis, Department of Electrical Engineering and Computer Science, MIT, September 1997.

18 H.A. Haus and Y. Silberberg, "Laser Mode Locking with Addition of Nonlinear Index," *IEEE J. Quantum Electron.* QE-22: 325 (1986); F.X. Kärtner, D. Kopf, and U. Keller, "Solitary-pulse Stabilization and Shortening in Actively Mode-locked Lasers," *J. Opt. Soc. Am. B* 12: 1927 (1996).

19 D.J. Kuizenga and A.E. Siegman, "FM and AM Mode Locking of the Homogeneous Laser. Part I: Theory," *IEEE J. Quant. Electron.* 6: 694 (1970).

20 G.R. Huggett, "Modelocking of CW Lasers by Regenerative rf Feedback," *Appl. Phys. Lett.* 13: 168 (1968); M. Nakazawa, E. Yoshida, and Y. Kimura, "Ultrastable Harmonically and Regeneratively Modelocked Polarization-Maintaining Erbium Fiber Laser," *Electron. Lett.* 30: 1603 (1994).

21 M. Nakazawa, K. Tamura, and E. Yoshida, "Supermode Noise Suppression in a Harmonically Modelocked Fibre Laser by Self-phase Modulation and Spectral Filtering," *Electron. Lett.* 32: 461 (1996).

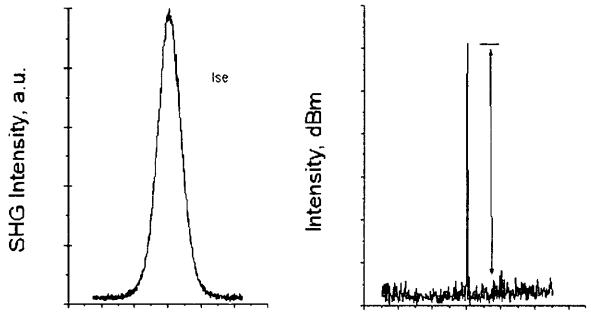

Figure 3. Autocorrelation and rf spectrum of the laser output.

One of the challenges to maintaining active modelocking is uncontrolled detuning between the intracavity modulator and the laser cavity harmonic. Temperature variations cause a change in the effective length of the fiber, leading to a change of the repetition rate of the laser relative to that of the modulator. The allowable detuning between the modulator and the cavity harmonic is on the order of tens of kilohertz. Without correcting for detuning, it has been observed in the lab that modelocking is lost after only a few minutes of operation. To correct for detuning in the laser, we have constructed a regenerative[22] scheme. The key element of the regenerative scheme is the clock extraction circuit (CEC)—comprised of a photodetector, amplifier, filter, and a phase shifter—that regenerates the signal driving the modulator from the harmonics of the laser itself. We have shown that employing the CEC ensures that the laser remains modelocked indefinitely. Future work includes stabilizing the laser with active control of the cavity length to achieve repetition-rate stability in the effort to build a truly clock-synchronized laser source.

Thesis

Grein, M.E. *A Regeneratively Modelocked, Fiber Ring Laser.* M.S. thesis, Department of Electrical Engineering and Computer Science, MIT, September 1997.

1.5 Asynchronous Phase-Modulated Optical Fiber Buffer

Sponsors

Defense Advanced Research Projects Agency
U.S. Air Force - Office of Scientific Research

Project Staff

David J. Jones, Dr. Katherine L. Hall, Professor Hermann A. Haus, Professor Erich P. Ippen

We demonstrated successful loading, storage, and unloading of 5 Gbit/sec packets from an asynchronous phase-modulated optical fiber ring buffer.[23] The asynchronous mode of operation[24] offers several practical advantages over synchronous operation[25] including tolerance of drifts in cavity length and loaded packet characteristics as well as possible elimination of clock recovery on incoming packets.

In essence, an optical fiber buffer of this type is an actively modelocked fiber ring laser that is held below threshold so that pulses cannot be spontaneously created. However, if pulses, seeded by "ones" in an input packet, are able to build up and suppression of "zeros" is maintained, the buffer can successfully store the packet. Viewed in this light, it is not surprising that loading of packets into the buffer induces relaxation oscillations (RO) that modulate the packet intensity as it circulates around the cavity. The time constant of the RO is the geometric mean of the upper-state lifetime of the erbium-dopant (in the silica host) and the photon lifetime in the resonator and equals approximately 10 ms. The detrimental effects of RO have limited the storage of previous optical fiber ring buffers to 20 ms.

The variation in the average power of the circulating packets, due to RO, can be minimized by optically injecting a CW holding beam. With this technique, either the packet or a CW signal is launched into the buffer. By correctly adjusting the power of the CW signal relative to the average packet power, the injected photon number is conserved, thereby inhibiting any RO. In this experiment a holding beam is

22 M. Nakazawa, K. Tamura, and E. Yoshida, "Supermode Noise Suppression in a Harmonically Modelocked Fibre Laser by Self-phase Modulation and Spectral Filtering," *Electron. Lett.* 32: 461 (1996).

23 D.J. Jones, K. L. Hall, H.A. Haus, and E.P. Ippen, "Asynchronous Phase-Modulated Optical Fiber Ring Buffer," *Opt. Lett.* 23: 177 (1998).

24 C.R. Doerr, H.A. Haus, and E.P. Ippen, "Asynchronous Soliton Mode Locking," Opt. Lett. 23: (1958); H.A. Haus, D.J. Jones, E.P. Ippen, and W.S. Wong, "Theory of Soliton Stability in Asynchronous Modelocking," *J. Lightwave Technol.* 14: 622 (1996).

25 C.R. Doerr, W.S. Wong, H.A. Haus, and E.P. Ippen, "Additive Pulse Mode-Locking/Limiting Storage Ring," *Opt. Lett.* 19: 1747 (1994).

generated by a gain-switched semiconductor laser which is injected into the buffer when packets are not present. Incorporating the holding beam led to significantly enhanced storage times of least 157 ms (1600 circulations). Limitations with our diagnostic equipment prevented us from observing storage beyond this limit.

Although we observed storage of the packet envelope for at least 157 ms, it is important to verify maintenance of the individual bits in the packet. A 10 bit portion of the loaded packet displayed on a 50 GHz sampling scope is given in Figure 4a, while Figure 4b shows the same 10 bit portion after 450 roundtrips (a storage time of 44.3 ms). To obtain the trace in Figure 4b, the sampling scope is triggered at the loading event and the delay is set to 44.3 ms. The apparent widening of the pulses in Figure 4b is caused by oscilloscope timing jitter due to the long time delay after the trigger event. Similar pulse broadening is observed on a trace taken directly of the packets with a 45 ms trigger delay, confirming oscilloscope jitter as the source. In addition, the sampling scope failed to hold its trigger beyond this point, preventing us from obtaining a packet trace past a storage time of 44.3 ms.

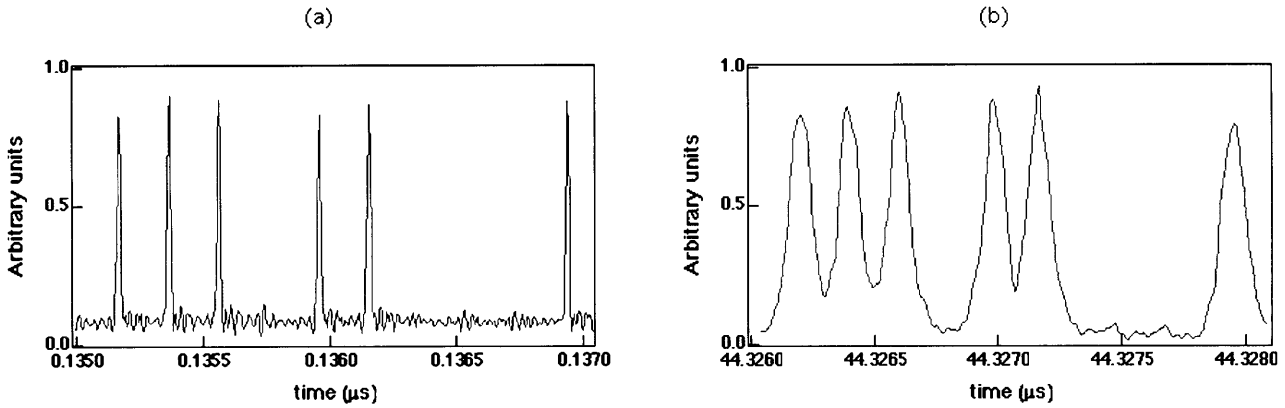

Figure 4. High-speed sampling scope trace showing a portion of (a) the initial, loaded packet; (b) after the 450 circulations. Pulse broadening in the stored packet is caused by jitter from the sampling oscilloscope.

1.6 Optical Pulse Filtering with Dispersion-Imbalanced Loop Mirrors

Sponsors

Defense Advanced Research Projects Agency
Joint Services Electronics Program
National Science Foundation
U.S. Air Force - Office of Scientific Research

Project Staff

William S. Wong, Shu Namiki, Dr. Mordehai Margalit, Professor Erich P. Ippen, Professor Hermann A. Haus, Dr. Per P. Hansen,[26] Dr. Torben N. Nielsen[27]

The nonlinear optical loop mirror (NOLM)[28] and the nonlinear amplifying loop mirror (NALM)[29] have been shown to possess optical switching properties[30] when they are imbalanced by an asymmetric coupler and by an asymmetrically placed gain element, respectively. They can be applied in a number of applications such as all-optical demultiplexing of data streams[31] and passive modelocking of short-pulse fiber lasers.[32]

We have demonstrated experimentally the possibility of constructing a new nonlinear optical Sagnac loop that is imbalanced by dispersion.[33] The response of this loop is significantly different from those of NOLMs and NALMs—since dispersion acts only on

26 Bell Laboratories, Lucent Technologies, Holmdel, New Jersey.

27 Ibid.

28 N.J. Doran and D. Wood, "Nonlinear-optical Loop Mirror," *Opt. Lett.* 13: 56 (1988).

29 M.E. Fermann, F. Haberl, M. Hofer, and H. Hochreiter, "Nonlinear Demonstration of Optical Soliton Switching in an All-fiber Nonlinear Sagnac Interferometer," *Opt. Lett.* 14: 754 (1990).

30 K.J. Blow, N.J. Doran, and B.K. Nayar, "Experimental Demonstration of Optical Soliton Switching in an All-fiber Nonlinear Sagnac Interferometer," *Opt. Lett.* 14: 754 (1989).

pulses, cw input light of arbitrary intensity is reflected while short pulses are switched out. Our idea is to construct the loop, as shown in Figure 5a, with one segment of fiber of high anomalous dispersion D_1, and another segment with a much lower amount of dispersion D_2. In the clockwise-propagating direction inside the loop mirror, the $N < 1$ (N is the soliton order) incident pulse disperses quickly and then remains broad in the second segment, inducing little nonlinear phase shift; on the other hand, the counter-clockwise-propagating pulse remains short for the entire first segment where the fiber is almost dispersionless, thus acquiring a large amount of nonlinear phase shift that is both intensity-dependent and proportional to L_2 (Figure 5b). It is important to note that such nonreciprocal phase shift exists for pulsed input but not for cw input. In other words, the dispersion-imbalanced loop is a nonlinear pulse filter that responds not to a dc input intensity, but rather to the second derivative of the electric field envelope u with respect to time.

The input and transmitted optical spectra are measured and shown in Figure 6. The extinction (loss) for cw in the output, relative to that of the pulse output, is 22 dB. Moreover, the pulse spectrum is modified in a favorable way—the spectral width broadens from 9 nm to 14 nm, while the resonant solitonic sidebands are rejected by the loop, resulting in a shorter and cleaner pulse after propagation in a DCF fiber. As shown in Figure 7, the output FWHM pulse width is compressed to 230 fs after 2.5 m of DCF, assuming a sech shape (time-bandwidth-product = 0.40). The suppression of the pedestal due to cw is evident in the log plot of the pulse autocorrelations before and after the loop.

In collaboration with Lucent Technologies in Holmdel, New Jersey, we also demonstrated the possibility of using a dispersion-imbalanced loop mirror to perform nonlinear noise filtering on a 10 Gb/s noise-loaded pulse stream.[34] In a fiber-optic communication system with in-line optical amplifiers, it is the presence of amplified spontaneous emission (ASE) noise in the signal stream that lowers the signal-to-noise ratio of the signal at the optical receiver, resulting in a higher bit error rate in transmission. By removing the in-band ASE noise, the resulting receiver sensitivity is improved from –37.0 dBm to –37.7 dBm. The experiment setup is shown in Figure 8. A 10 GHz pulse train, where the 15 ps pulses have a time-bandwidth-product of 0.35 at 1550 nm, is modulated at 10 Gb/s by a lithium niobate amplitude modulator with a 2^{31}-1 pseudo-random bit sequence. The noise source consists of two erbium-doped amplifier stages in cascade, into which a 1 nm band-pass filter is inserted between the two stages to lower the noise bandwidth and increase the noise spectral power simultaneously. As a result, 8.3 dBm of ASE noise is generated at the signal wavelength with a bandwidth of 1.3 nm. The signal and the ASE noise are both launched into the loop mirror via a 50/50 coupler followed by a three-port optical circulator. The dispersion-imbalanced loop mirror is constructed with a 50/50 coupler, 12.62 km of Lucent TrueWave fiber with an anomalous dispersion of +3.52 ps/(nm.km), and 11.36 km of TrueWave fiber with an anomalous dispersion of +1.68 ps/(nm · km) at 1550.0 nm.

31 D.M. Patrick, A.D. Ellis, and D.M. Spirit, "Bit-rate Flexible All-Optical Soliton De-multiplexing using a Nonlinear Optical Loop Mirror," *Electron. Lett.* 29: 702 (1993). K. Uchiyama, H. Takara, T. Morioka, S. Kawanishi, and M. Saruwatari, "100 Gbit/s Multiple-channel Output All-optical Demultiplexing based on TDM-WDM Conversion in a Nonlinear Optical Loop Mirror," *Electron. Lett.* 32: 1989 (1996).

32 I.N. Duling, III, "Subpicosecond All-fibre Erbium laser," *Electron. Lett.* 27: 544 (1991); D.J. Richardson, R.I. Laming, D.N. Payne, V. Matsas, and M.W. Phillips, "Self-starting, Passively Modelocked Erbium Fibre Ring laser Based on the Amplifying Sagnac Switch," *Electron. Lett.* 27: 542 (1991); S. Wu, J. Strait, and R.L. Fork, "High-power Passively Mode-locked Er-doped Fiber Laser with a Nonlinear Optical Loop Mirror," *Opt. Lett.* 18: 1444 (1993).

33 W.S. Wong, S. Namiki, M. Margalit, E.P. Ippen, and H.A. Haus, "Optical Pulse Filtering with Dispersion Imbalanced Nonlinear Loop Mirrors," OFC '97 postdeadline paper PD-8, Dallas, Texas, 1997; W.S. Wong, S. Namiki, M. Margalit, E.P. Ippen, and H.A. Haus, "Self-switching of Optical Pulses in Dispersion-imbalanced Nonlinear Loop Mirrors," *Opt. Lett.* 22: 1150 (1997).

34 W.S. Wong, P.B. Hansen, T.N. Nielsen, M. Margalit, S. Namiki, E.P. Ippen, and H.A. Haus, "In-band Amplified Spontaneous Emission Noise Filtering with a Dispersion-imbalanced Nonlinear Loop Mirror," submitted to *J. Lightwave Technol.*

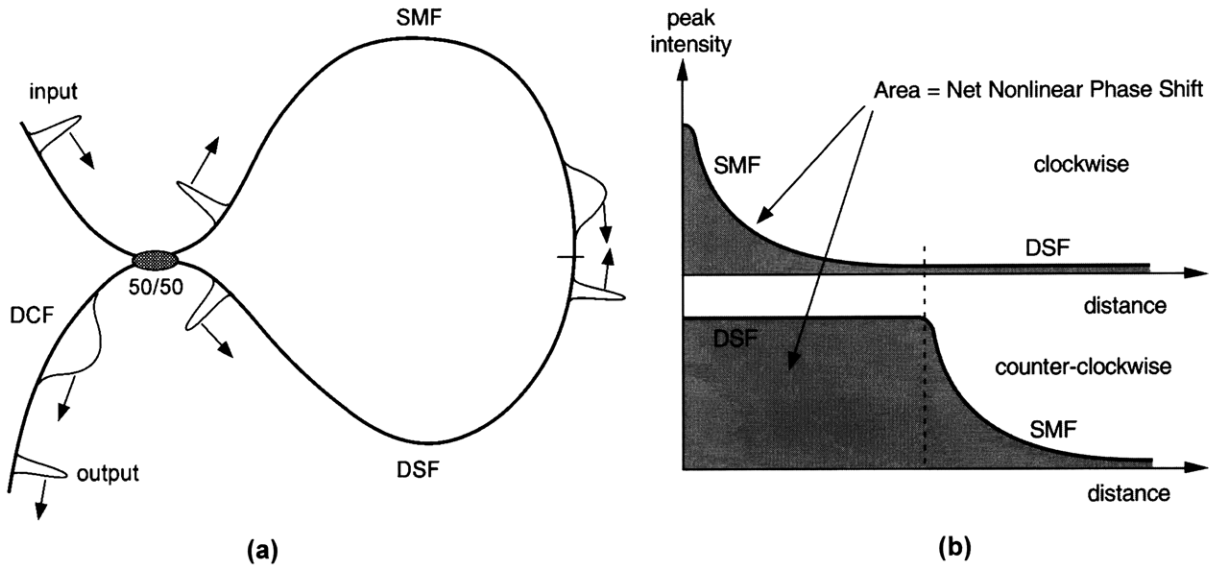

Figure 5. (a) Conceptual operation of a dispersion-imbalanced loop mirror showing pulse stretching and compression. (b) Plots of the pulse peak intensity as a function of distance along the two propagation directions.

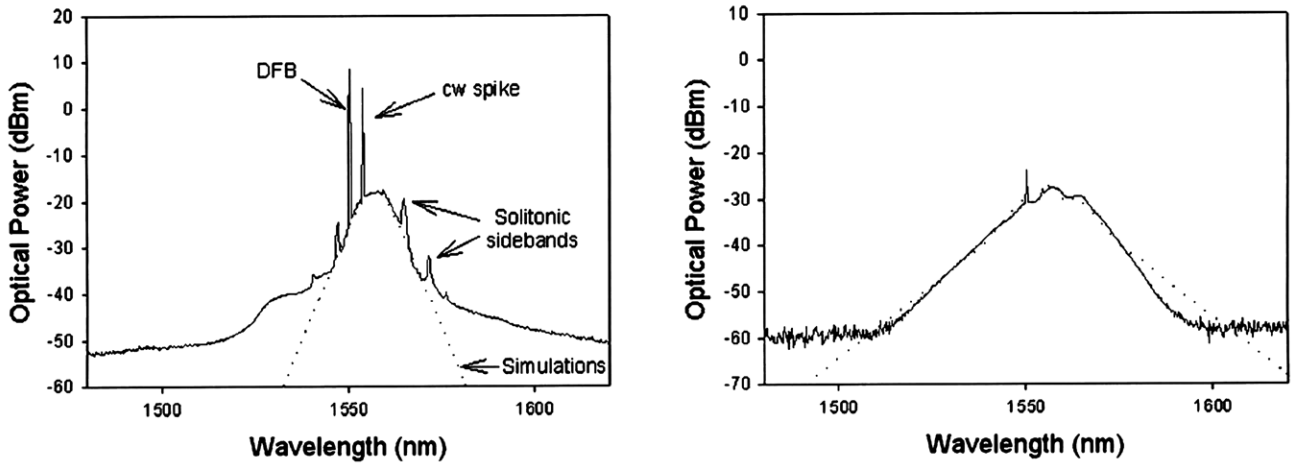

Figure 6. Input and output optical spectra.

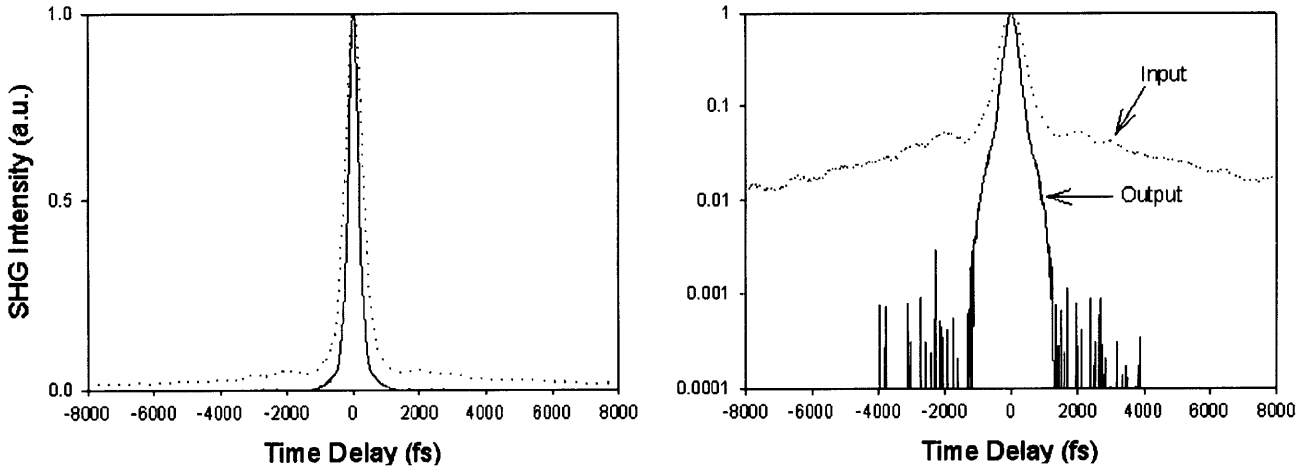

Figure 7. Autocorrelations of the input pulse (τ_{FWHM} = 230 fs).

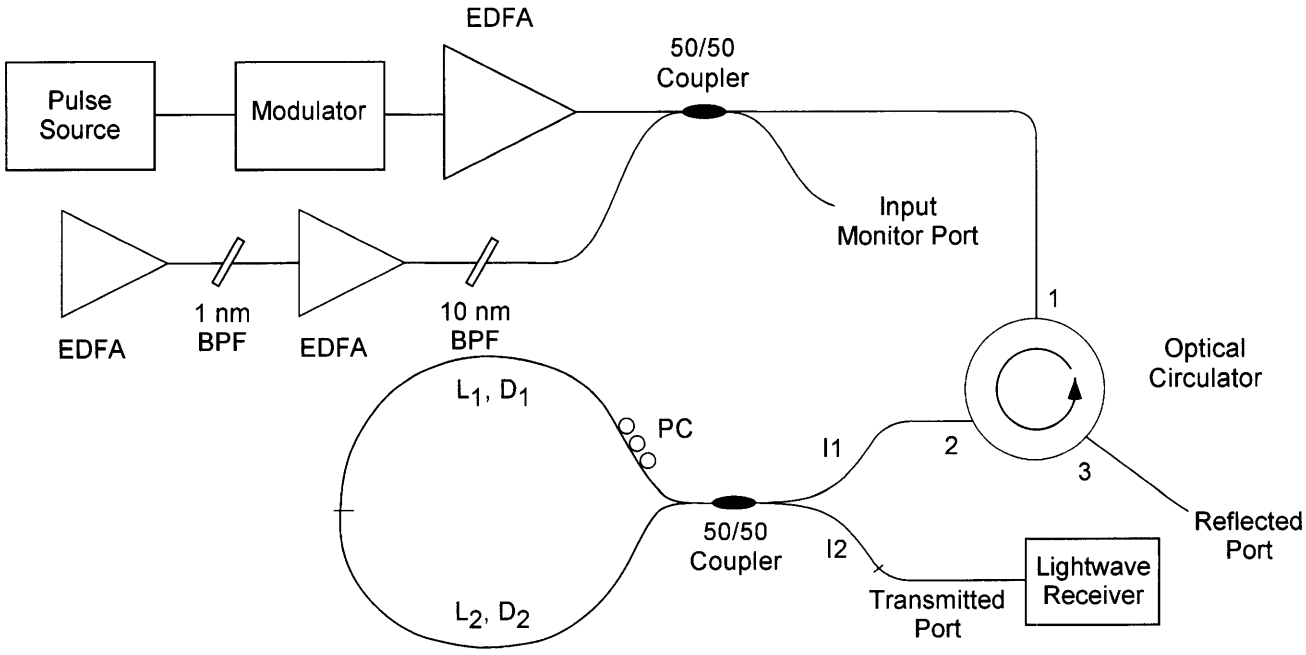

Figure 8. Experimental setup: PC, polarization controller; EDFA, erbium-doped fiber amplifer; BDF, band-pass filter.

For pulse input without noise injected, the transmitted power as a function of input power is measured and shown in Figure 9. The switching energy corresponding to the first peak is 4 pJ, and the output FWHM pulse width is shortened to 9 ps at that point. The agreement with numerical simulations, computed with a split-step Fourier algorithm, is good. The input and the transmitted signal through the loop mirror are both fed to an optically pre-amplified lightwave receiver for bit error rate measurements. Without noise loading, the measured BERs through the loop mirror at 28 mW of input power are shown in Figure 10 as circles. When compared to the BERs without the loop mirror (squares), one can see that the insertion of the loop mirror causes no penalty in receiver sensitivity. Furthermore, when in-band ASE noise is added to the system such that the input optical signal-to-noise ratio decreases from 38 dB to 15 dB in 0.2 nm of bandwidth, the degraded sensitivity

of -37.0 dBm measured without the loop mirror (triangles) can be improved to -37.7 dBm (inverted triangles).

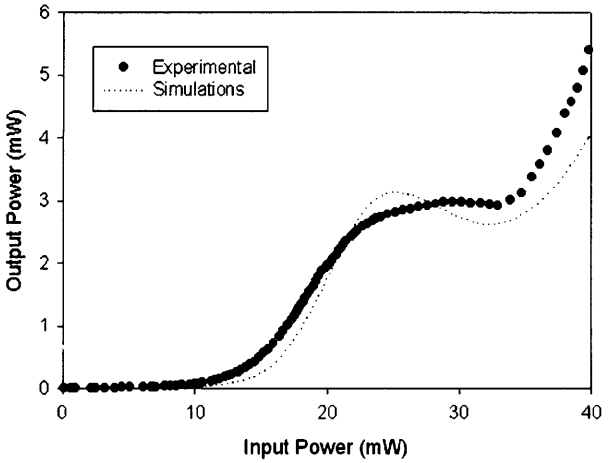

Figure 9. Switching characteristics of the dispersion-imbalanced loop mirror.

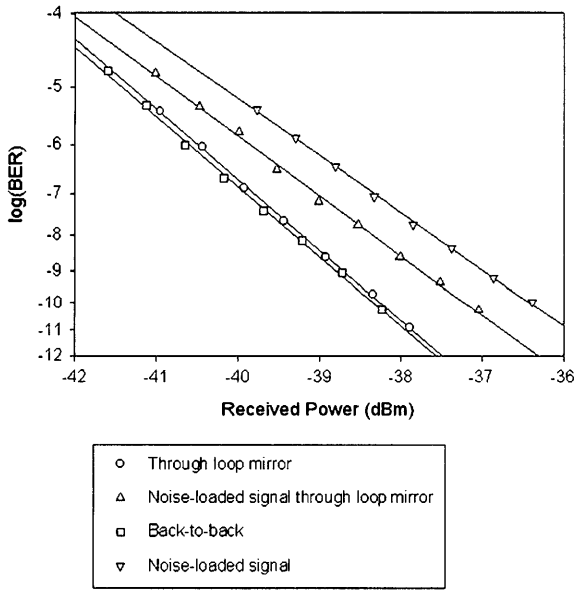

Figure 10. Measured bit error rate curves as a function of power received at the receiver.

1.6.1 Publications

Wong, W.S., S. Namiki, M. Margalit, E.P. Ippen, and H.A. Haus. "Optical Pulse Filtering with Dispersion Imbalanced Nonlinear Loop Mirrors." OFC '97 postdeadline paper PD-8, Dallas, Texas, 1997.

Wong, W.S., S. Namiki, M. Margalit, E.P. Ippen, and H.A. Haus. "Self-switching of Optical Pulses in Dispersion-imbalanced Nonlinear Loop Mirrors." *Opt. Lett.* 22: 1150 (1997).

1.7 Stretched-Pulse Propagation

Sponsor

U.S. Air Force - Office of Scientific Research

Project Staff

Professor Hermann A. Haus, Dr. Masayuki Matsumoto

Linear non-return-to-zero (NRZ) long-distance communications without repeaters has been in place since 1995. Competing nonlinear soliton communications has not yet won a competitive edge for the following reasons:

1. Long distance soliton communication systems have been based on the sliding guiding filter principle.[35] Whereas the performance of these systems is greatly superior to the "linear" approach, the sliding guiding filters require different filters in different amplifier pods. This feature seems unacceptable to system engineers.
2. NRZ can span the Pacific with a bit-rate of 5 Gbit/s and allows expansion with wavelength division multiplexing.

However, nonlinear schemes of propagation accommodate, to a great extent, the nonlinear properties of fibers and allow for a higher S/N ratio. We have been studying the propagation of pulses of high intensity in systems of alternating negative and positive dispersion fiber segments.[36] The pulses alternately stretch and compress within each "cell" of a pair of positively and negatively dispersive fiber segments. In this respect, the propagation is similar to the propagation of pulses within the passively modelocked stretched pulse laser.[37] The stretched pulse laser operates via self-phase modulation, self-amplitude modulation, filtering and group velocity dispersion. In stretched pulse communications there is no need for self-

35 L.F. Mollenauer, J P. Gordon, and S.G. Evangelides, "The Sliding Frequency Guiding Filter: an Improved form of Soliton Jitter Control," *Opt. Lett.* 17: 1575 (1992).

36 M. Matsumoto and H.A. Haus, "Stretched-pulse Optical Fiber Communications," *IEEE Photonics Technol. Lett.* 9: 785 (1997).

amplitude modulation required in a laser for pulse stability against noise build-up. Stretched pulse propagation can occur in the regime of negative as well as positive average dispersion. In the latter case, the pulses are chirped. The scheme has several advantages.

1. The average dispersion can be set by adjustment of the individual fiber segment lengths and is not determined by the availability of fiber of a particular dispersion characteristic. The average dispersion can be set at a much lower value than could be achieved with uniform fiber under existing fabrication tolerances. Small dispersion reduces the Gordon-Haus jitter[38] and thus it is possible to attain acceptable transmission characteristics even without sliding guiding filters.
2. The average dispersion can be positive as well. This permits channel distributions over a wider bandwidth than would be possible if propagation were limited to net negative dispersion.
3. Since the pulses are not solitons and are chirped, phase matching to sidebands of perturbations due to periodic amplification is reduced, permitting a greater (more than triple) amplifier spacing than that of soliton systems.

We are pursuing the study of these systems in particular with respect to pulse collisions on bit-error rates of wavelength division multiplexed systems.

1.7.1 Publication

Matsumoto, M., and H.A. Haus. "Stretched-Pulse Optical Fiber Communications." *IEEE Photonics Technol. Lett.* 9: 785 (1997).

1.8 Direct Measurement of Self-Phase Shift due to Fiber Nonlinearity

Sponsors

National Science Foundation
U.S. Air Force - Office of Scientific Research
U.S. Navy - Office of Naval Research

Project Staff

Dr. Mordehai Margalit, Charles Yu, Professor Hermann A. Haus, Professor Erich P. Ippen

Many nonlinear optical experiments utilize glass fiber. One of the most important nonlinear effects experienced by a pulse propagating through the fiber is the accumulation of a nonlinear phase shift. Thus, this nonlinear phase shift is a good measure of the fiber nonlinearity. Moreover, for some experiments this phase directly controls the experimental outcome.[39] Knowledge of the nonlinear phase shift is essential. Most previously used measurement techniques only characterize the dynamic phase within the pulse and do not determine the absolute phase shift.

We have devised a novel method to measure this phase shift based on spectral interferometry (SI).[40] SI measures the sum spectrum of a reference and a signal that are coherent and separated in time by t. The beating between signal and reference generates a sinusoid in frequency whose period is the inverse of the temporal separation t. We ensure that only the signal, not the reference, is affected by the fiber nonlinearity. So the nonlinear phase imposed on the signal distorts the signal-reference beating sinusoid. Near the center of the spectrum the distortion is manifested by a shift of the beating pattern, and the shift is a direct measure of the phase at the peak wavelength. We have shown numerically that it approximates well the nonlinear phase shift at the temporal peak of the pulse.

37 H.A. Haus, K. Tamura, L.E. Nelson, and E.P. Ippen, "Stretched Pulse Additive Pulse Mode-Locking in Fiber Ring Lasers; Theory and Experiment," *J. Quant. Electron.* 31: 1-8 (1995).

38 J.P. Gordon and H.A. Haus, "Random Walk of Coherently Amplified Solitons in Optical Fiber Transmission," *Opt. Lett.* 11: 665-67 (1986).

39 K. Bergman and H.A. Haus, "Squeezing in Fibers with Optical Pulses," *Opt. Lett.* 16: 663 (1991); W. Wong, S. Namiki, M. Margalit, H.A. Haus, and E.P. Ippen, "Self-Switching of Optical Pulses in Dispersion-Imbalanced Nonlinear Loop Mirrors," *Opt. Lett.* 22: 1150 (1997).

40 C. Froehly, A. Lacourt, and J. Vienot, "Time Impulse Response and Time Frequency Response of Optical Pupils: Experimental Confirmations and Applications," *J. Opt. (Paris)* 4: 183 (1973).

We have implemented this technique in an experiment using 1.7 km of fiber. We tuned our optical source so that the fiber dispersion was negative or positive depending on the wave-length of the optical signal. We observed that for the positive dispersion case the spectrum broadens as the input power increases. The nonlinear phase shift also increases linearly with input power. For the negative dispersion case, the spectrum narrows as the input power increases because of soliton effects. The nonlinear phase shift also increases initially. However, when the soliton condition is reached, both the spectral bandwidth and the nonlinear phase shift stay the same. This is because an increase of the input power beyond the soliton limit generates continuum and does not contribute to the soliton energy.

These experimental observations agree well with our theoretical calculations and numerical simulations. Figure 11 shows some of the experimental results. Figure 11a shows the optical spectrum of the pulse pair before and after the fiber when dispersion is negative. Figure 11b shows the same spectra on an expanded 1 nm scale. The fringes are uniform and the phase shift can be easily deduced. Figure 11c and Figure 11d show the spectra for the positive dispersion case with different spans. The fringes are again uniform. This technique is easy to implement and very accurate. We expect it to be a useful diagnostic tool for many nonlinear fiber experiments.

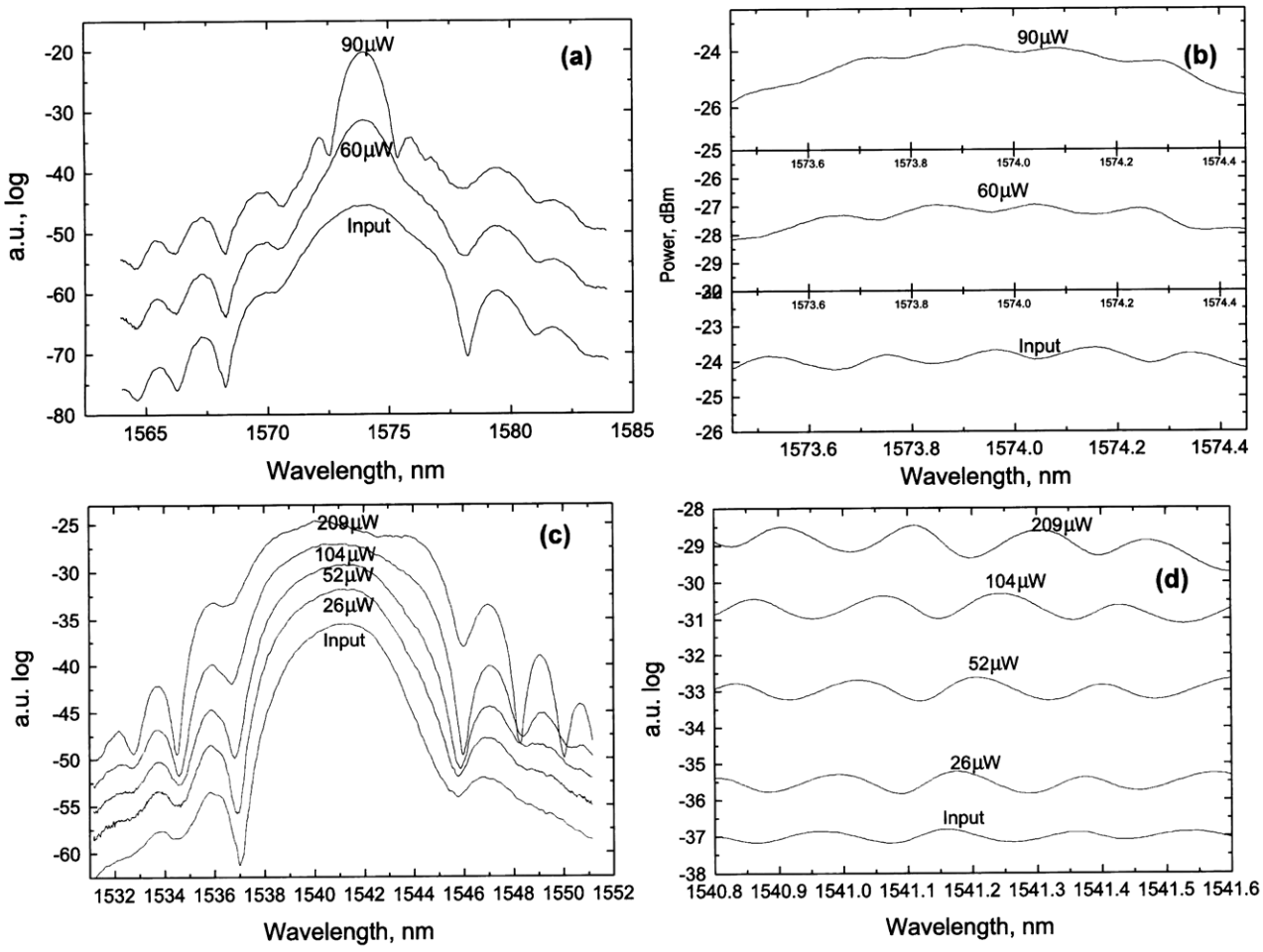

Figure 11. (a) Spectra before and after fiber, 20 nm span; (b) Spectra before and after fiber, 1 nm span for different powers, negative dispersion case; (c) Spectra before and after the fiber, 20 nm span; (d) Spectra before and after fiber, 1 nm span for different powers, positive dispersion case.

1.9 Wavelength Stabilized Modelocked Laser Source Gyro Applications

Sponsor

Charles S. Draper Laboratory

Project Staff

Patrick C. Chou, Dr. Oldrich M. Laznicka, Professor Hermann A. Haus

We are investigating techniques for generating optical radiation suitable for exciting a high-performance fiberoptic gyroscope and other fiber-based sensors. An ideal source would be continuous wave, high power, very low in coherence, and with a mean wavelength stable to better than a part per million. Low coherence is necessary to minimize errors due to backscattering. Since measurements can occur over periods of days or weeks, wavelength stability is required because the measured signal must not drift over that time.

The conventional scheme uses a superluminescent diode, in which it is difficult to achieve high power and low coherence simultaneously, especially at 1.55 μm where superluminescent diode technology is relatively undeveloped. The basis of our optical source is a stretched pulse fiber laser, which is attractive because of its wide optical bandwidth and relatively high power. The wide bandwidth translates into low coherence. This laser has high power output, unlike the superluminescent diode which tends to narrow in bandwidth as power is increased.

One drawback to the stretched pulse fiber laser is that its output pulses have very high peak intensity and result in errors due to optical nonlinearity in the fiber of the gyro coil. We have shown that this can be alleviated by properly preparing the pulses before they enter the gyro. One must send them through a highly dispersive medium so that the pulse widths become so long that they overlap each other. It may also be necessary to scramble the phases of the pulses to prevent beats.

Mean wavelength stabilization is also a critical issue. Stabilizing a broadband optical source is different from the more common problem of stabilizing a single frequency laser. First, one must accurately sense the mean wavelength, analogous to the center of mass of the spectrum. A compact and stable device to measure this quantity is currently being custom manufactured in a glass waveguide structure. Second, one must be able to control the mean wavelength. Since we are working with chirped pulses, we can take advantage of the fact that the different frequencies of a chirped pulse are spread out over time. We can then control the optical spectrum by modulation in the time domain.

For the fibergyro application, low-frequency noise is also an issue because the detection schemes incorporate modulation at frequencies from 100 kHz to a few MHz. It is not clear yet whether it is easier to build a high-power, low-noise pulse source or an amplified low-power, low-noise source. We are currently investigating both cases.

1.10 Optical Measurements of Photonic Bandgap Resonators in the Near Infrared

Sponsors

National Science Foundation/MRSEC

U.S. Air Force – Office of Scientific Research

Project Staff

Daniel J. Ripin, Dr. Brent E. Little, Dr. Günter Steinmeyer, Erik R. Thoen, Professor Erich P. Ippen

Photonic bandgap crystals (PBGs) are periodic lattices comprised of materials with very different dielectric constants. These crystals can be used for the basic manipulation and control of light, similar to the ways that electronic crystals manipulate electrons. With the addition of defects, photonic crystals can confine light to dimensions on the order of its wavelength. One-dimensional dielectric structures utilizing these unique properties have been designed to serve as narrow bandpass wavelength filters. The basic design is an optical ridge waveguide with evenly spaced air holes. A defect in the spacing between two of the holes is introduced to create a high-Q cavity. Light on resonance with the cavity is transmitted, while all other wavelengths are reflected. Structures with this design have been fabricated in two material systems, Si/SiO_2 and $GaAs/Al_xO_y$. Filters in the proper wavelength regime have the potential to be applied as channel dropping filters for WDM, or as components of integrated photonic chip devices.

We have characterized various devices designed and fabricated in collaboration with the groups of Professors Joannopoulos, Kimerling, Kolodziejski, and Smith and observed for the first time a PBG res-

onance in the near IR. A cw tunable NaCl F-center laser was used for the transmission measurements. This laser is tunable from 1510 nm to 1680 nm, with an average output power of 250 mW. The light is coupled into small ridge waveguides with dimensions 0.2 x 0.5 μm using an optical fiber with a lensed output tip. Figure 12 shows the transmission measured through the PBG device in the silicon system.[41] The resonance is at 1560 nm, within 1% of the calculated value 1547 nm, and has a quality factor of 265. The modal volume was calculated to be 0.055 μm^3. By using structures with scaled hole dimensions, we were able to observe the band edges of the gap. A shift was then calculated to put the band edges on the same plot as the resonance, giving excellent agreement with theory.

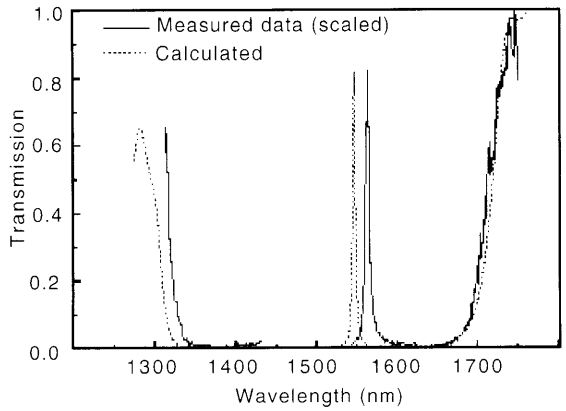

Figure 12. Comparison of measured transmission (solid lines) to calculated transmission (dotted line) for a PBG microcavity with four holes on each side of the microcavity. The upper-band and lower-band edge transmission data have been shifted in wavelength according to hole dimension scaling.

Using the same experimental setup, we have also studied transmission through ring resonators, a promising alternative to PBG devices for wavelength filtering. The ring resonator, two high dielectric contrast waveguides side-coupled to a circular ring waveguide, was also manufactured in the silicon material system and measured.[42] The waveguide dimensions are the same as above but are fabricated with polycrystalline silicon. These waveguides were measured to have scattering losses around 20 dB/cm. The fabricated rings have radii ranging from 3 to 5 mm. Several resonances were observed near 1550 nm with a quality factors up to 250 and free spectral ranges (FSR) as large as 24 nm. The depths of the nulls were measured to be deeper than 15 dB down from the off-resonance values.

PBG devices using GaAs structures are also being fabricated in Professor Kolodziejski's laboratory. These devices include air-bridge structures as well as the ridge geometry discussed above. In air-bridge crystals, the PBG is suspended over air, which will increase the dielectric contrast between the guide and surrounding material and produce even tighter resonator mode confinement. Coupling to these bridges and waveguide transmission losses is being investigated experimentally. New experiments are also underway to further develop the ring resonator technology.

1.10.1 Publication

Foresi, J.S., P.R. Villeneuve, J. Ferrera, E.R. Thoen, G. Steinmeyer, S. Fan, J.D. Joannopoulos, L.C. Kimerling, H.I. Smith, and E.P. Ippen. "Photonic-Bandgap Microcavities in Optical Waveguides." *Nature* 390: 143 (1997).

1.11 Optical Resonant Structures

Sponsors

Defense Advanced Research Projects Agency
National Science Foundation/MRSEC

Project Staff

Mohammad Jalal Khan, Christina Manolatou, Dr. Jay N. Damask, Dr. Shan-Hui Fan, Dr. Brent E. Little, Professor Hermann A. Haus

We are investigating the design and modeling of resonant structures for use as channel dropping filters that are key components for WDM. These filters access one particular channel of a WDM signal without disturbing other channels. The linewidth of channel dropping filters must be wide enough to accommodate the bandwidth of the individual channels (about 10 GHz) but also narrow enough to avoid cross talk from adjacent channels (spaced about 100 GHz apart). In order to accommodate the full band-

41 J.S. Foresi, P.R. Villeneuve, J. Ferrera, E.R. Thoen, G. Steinmeyer, S. Fan, J.D. Joannopoulos, L.C. Kimerling, H.I. Smith, and E.P. Ippen, "Photonic-Bandgap Microcavities in Optical Waveguides," *Nature* 390: 143 (1997).

42 B.E. Little, J.S. Foresi, G. Steinmeyer, E.R. Thoen, S.T. Chu, H.A. Haus, E.P. Ippen, L.C. Kimerling, W. Greene, "Ultra-Compact Si/SiO_2 Microring Resonator Optical Channel Dropping Filters," *IEEE Photonic Tech. Lett.*, forthcoming.

width of the erbium doped fiber amplifiers (about 40 nm around the 1550 nm optical wavelength) these filters must also have large free spectral range (FSR).

Resonant structures can achieve very narrow linewidths for a given device size and can be combined together to further modify the Lorentzian response of a single resonator yielding higher order filters. Placed between a bus and a receiver waveguide, they can tap off all the power of a particular channel from the bus, at the resonance frequency, and transfer it to the receiver. In order to satisfy the WDM system requirements the loaded, and the radiation Q's of the resonators should be of the order of 10^3 and 10^4, respectively, and their size should be small in order to achieve a large FSR. The use of resonators based on high index contrast structures may be a viable approach leading to device sizes only of the order of a few wavelengths.

We are investigating a type of channel dropping filter that employs degenerate symmetric and antisymmetric resonant modes. The simplest realization of the basic structure is a ring resonator. The ring supports two modes that can be described either in terms of circulating waves in opposite directions around the ring or in terms of standing waves. The main difficulty in the use of ring resonators is associated with the surface roughness of the ring waveguide walls, which, in addition to causing radiation loss, couples the two counter propagating traveling waves and degrades the performance.

The principle of operation of the ring resonator can be generalized to standing wave resonant structures with symmetry, such as a pair of mutually coupled identical standing wave resonators. When these modes are side-coupled to two waveguides, full power transfer can be achieved at resonance provided that the symmetric and antisymmetric modes have the same resonance frequency and quality factor.

Coupling of modes is our first approximation for analyzing the filter performance and for deriving an equivalent circuit which provides a correspondence with standard filter design techniques. This approach can further be used for design of multipole filters in the case that the 20 dB/decade roll-off of the single pole Lorentzian response is not adequate to meet the cross-talk specifications. (This is done by coupling several pairs of degenerate resonators; the coupling between the resonators is appropriately chosen to obtain the desired spectral response.)

A rough estimate can be obtained analytically, but the actual performance can only be determined from a full numerical solution of Maxwell's equations which includes the loading of the resonances. We use the finite difference time domain (FDTD) method to find the resonator modes, the radiation and loaded Q's, and the spectral response of the filter over a wide bandwidth for different material and geometrical parameters of the waveguides and resonators.

A square or rectangular dielectric structure is a very simple realization of a standing wave resonator. In such structures most of the radiation loss is expected at the corners, so a mode with a high Q should have nulls at the corners. Figure 13 shows the field computed using FDTD in a square resonator side coupled to a waveguide, after elapse of time so that the mode with the highest Q has survived. Of all the modes that are initially excited in the resonator by the waveguide field, the ones with high field intensity at the corners, soon radiate away leaving the mode of Figure 13 that has nulls along the diagonals of the square. The ultimate aim is to construct a degenerate symmetric and antisymmetric mode of two square or rectangular resonators via side-coupling to two waveguides as shown in Figure 14.

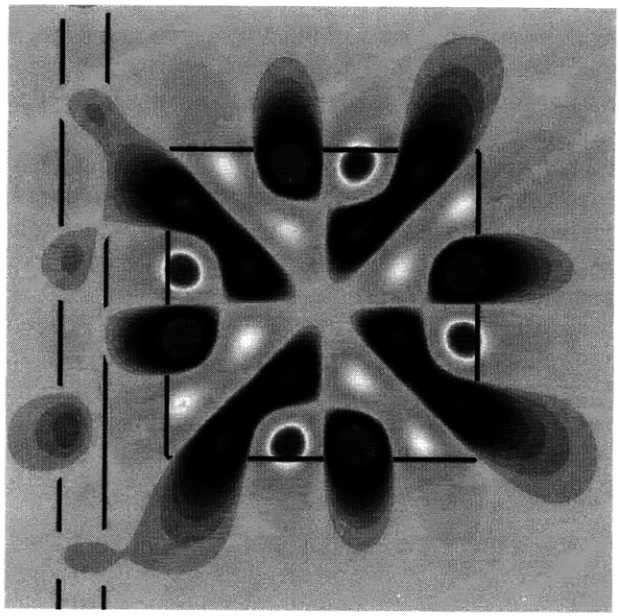

Figure 13. The electric field intensity of the mode of highest Q in a square cavity.

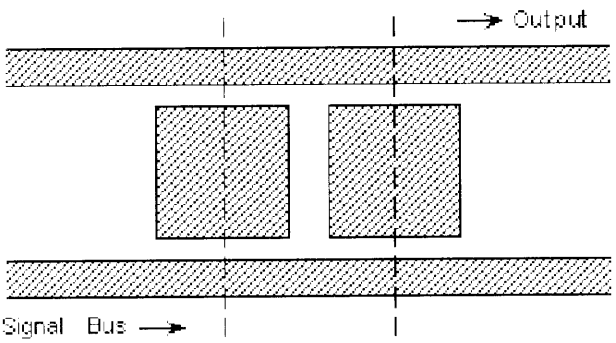

Figure 14. A coupled cavity channel drop- or add-filter.

1.12 Ultrafast Gain-Index Coupling in InGaAsP Diode Lasers

Sponsors

Joint Services Electronics Program
U.S. Air Force - Office of Scientific Research

Project Staff

Erik R. Thoen, Dr. Günter Steinmeyer, Po-Hsiu Cheng, Daniel J. Ripin, Dr. Katherine L. Hall, Dr. Joseph P. Donnelly, Professor Erich P. Ippen

Diode lasers and semiconductor optical amplifiers at telecommunication wavelengths are being used increasingly for high-speed data transmission, optical switching, four-wave mixing, and other nonlinear optical applications. A basic understanding of their nonlinear properties on ultrafast time scales is essential to define the limits of the current technologies and to define new applications. We have performed heterodyne pump-probe measurements to determine the ultrafast response of InGaAsP quantum well semiconductor optical amplifiers at 1.55 μm. A femtosecond optical parametric oscillator system has been used to study the wavelength dependence of the various contributions to the ultrafast response in these devices.

An experimental investigation of dynamic gain-index coupling in such amplifiers has been performed using simultaneous measurements of transmission and phase changes. Both gain and index dynamics are expected to contribute artifacts to each other's measurements proportional to the time derivative of the response and the spectral slope of the linear transmission function. Typical experimental traces of the apparent gain and index dynamics are shown in Figure 15. The deduced contribution of the dynamic coupling, shown by the dashed curve, qualitatively exhibits the expected dependences. The measurements suggest, however, that even when the gain-index coupling is accounted for, a delay in carrier heating is still a significant component in the gain response as indicated in our previous work.

Because our heterodyne technique is capable of both gain and index measurements, careful measurements of the alpha parameters associated with intraband density changes and interband carrier heating have been obtained as a function of current injection and wavelength. This is the first time that the alpha parameter associated with carrier heating has been measured as a function of wavelength in these devices.

Currently we are optimizing a fiber laser based upon the erbium-doped stretched-pulse fiber laser to be used for sub-100 femtosecond measurements of laser diodes. With such short pulses, the effect of dynamic gain-index coupling should be even more significant, and the time constant of carrier-carrier scattering can be more accurately measured.

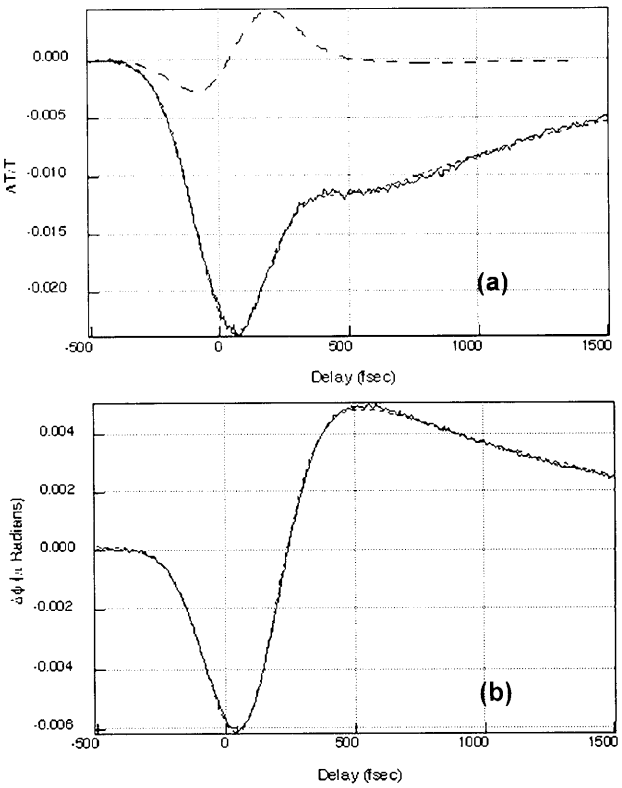

Figure 15. The measured gain (top) and index (bottom) response of an optical amplifier. In the top graphic, the dotted line is the extracted component of the gain response due to dynamic gain-index coupling.

1.13 Femtosecond Studies of THz Acoustic Phonons in PbTe Quantum Dots

Sponsors

Joint Services Electronics Program
U.S. Air Force - Office of Scientific Research

Project Staff

Erik R. Thoen, Gaston Tudury, Dr. Günter Steinmeyer, Daniel J. Ripin, Dr. Patrick Langlois, Professor Erich P. Ippen

Because of their strong quantum confinement, semiconductor quantum dots offer the potential of application as efficient nonlinear optical elements. Recently, their use for saturable absorber modelocking has been successfully demonstrated. Previous work on the nonlinear response of quantum dots has been mainly concentrated on cadmium-compound nanocrystals, which exhibit strong nonlinearities in the visible spectrum. The lower bandgap of lead compounds provides opportunity to produce quantum dots absorbing in the wavelength range from 1 to 2 μm, so they can be tailored to the gain spectra of virtually all solid state lasers in that range. Also, with their large bulk exciton Bohr radius, they allow strong quantum confinement with relatively large nanocrystals.

We are investigating the nonlinear transmission characteristics of PbTe quantum dot glasses (obtained through collaboration with C.L. Cesar of UNICAMP, Campinas, Brazil) with a high-sensitivity heterodyne pump-probe experiment. A femtosecond optical parametric oscillator system producing pulses of 130 fs, tunable from 1.35 to 1.6 μm, was used in these experiments. The nonlinear response of a quantum dot sample with an exciton peak at 1.365 μm excited with 1.5 μm pump beam is shown in Figure 16. It exhibits three components, a slow exponential decay with a response time of 70 ps, a fast response with a time constant in the range of 100 fs, and an oscillatory component with a frequency of 0.55 THz and damping time constant of about 2.5 ps. The frequency of these oscillations is clearly a signature of acoustic vibrations. To our knowledge, this is the first time that coherent acoustic phonons have been observed in quantum dots in a glass matrix.

Acoustic phonons in quantum dots have been analyzed theoretically by several authors. Using the bulk velocity of sound in PbTe, we calculate a resonance frequency of 0.4 THz for the fundamental breathing mode of a 4.3 nm unstrained quantum dot. This frequency agrees qualitatively with what is observed experimentally. We are in the process of investigating the wavelength dependence of the oscillations and the damping and relating them to the distribution, dephasing, and other loss mechanisms.

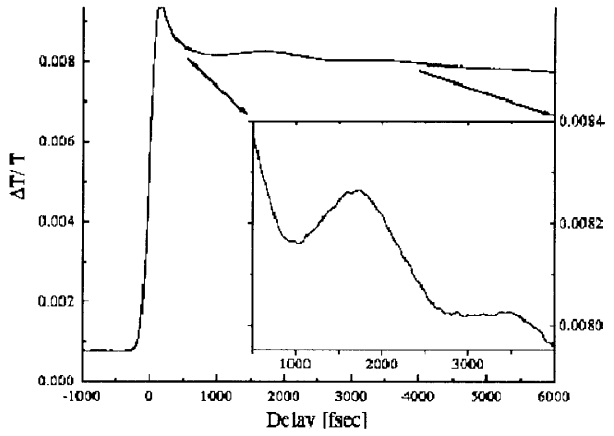

Figure 16. Transmission of the probe at 1.5 mm as a function of time through PbTe quantum dots in a glass matrix. The oscillations result from excitation of the spheroidal acoustic mode of the quantum dots.

1.14 Ultrashort Pulse Generation and Ultrafast Phenomena

Sponsors

Joint Services Electronics Program
Grant DAAH04-95-1-0038
U.S. Air Force - Office of Scientific Research
Contract F49620-95-1-0221
U.S. Navy - Office of Naval Research (MFEL)
Contract N00014-91-J-1956
Contract N000014-97-1-1066

Project Staff

Dr. Brett E. Bouma, Igor P. Bilinsky, Seong-Ho Cho, Boris Golubovic, Rohit Prasankumar, Professor Erich P. Ippen, Dr. James N. Walpole,[43] Leo J. Missaggia,[44] Dr. Victor P. Mikhailov,[45] Professor James G. Fujimoto

43 MIT Lincoln Laboratory, Lexington, Massachusetts.

1.14.1 Novel Modelocked Laser Cavity Designs For High-Peak Intensities

Ultrashort pulse sources are of fundamental importance for advances in signal processing, high speed communications, and investigation of ultrafast nonlinear processes in semiconductor materials and devices. Generally, these sources must be technologically simple, robust, and cost effective. In the last several years, significant advances have been made in the development of Kerr lens modelocking (KLM) utilizing electronic Kerr effect for fast saturable absorber action. KLM has allowed generation of the shortest pulses ever produced directly from a laser oscillator.[46] Working in collaboration with Professors Erich P. Ippen and Hermann A. Haus, we have developed a theoretical model which provides a foundation for understanding and optimizing short-pulse KLM lasers.[47]

Generation of femtosecond pulses with high intensities in the MW range is essential for a number of applications including optical harmonic generation and investigation of ultrafast nonlinear optical phenomena. The peak power directly generated by modelocked Ti:Al_2O_3 laser sources is in the range of 0.1 MW which is often insufficient for studies of nonlinear phenomena. Along with a traditional short pulse amplifier approach, our group has recently demonstrated the use of cavity dumping to increase output pulse peak power from a KLM Ti:Al_2O_3 laser.[48] Investigators have also examined techniques to design standard repetition rate KLM lasers to operate at high power and achieve high-intensity pulses.[49] The development of low cost, high intensity laser sources will enable a wider range of femtosecond measurement applications, making this technology more available to both the research and the development community.

We focused our efforts on designs that generate high intensity pulses directly from a modelocked laser oscillator without the need for amplification. Although these methods will not achieve pulse energies as high as those obtained using traditional short pulse amplifiers, they offer a significant advantage in cost and system complexity.

We developed a simple alternative method for improving peak power from a laser by designing a novel long cavity geometry for KLM. Our objective is to increase the laser output pulse energies and intensities by increasing laser cavity length. While keeping the laser average output power constant, the pulse energy can be increased by reducing the laser repetition rate. The development of long-cavity lasers requires careful design because the operation of KLM depends critically on laser cavity design. The laser cavity must be operated in a particular subset of its stability region in order to optimize modelocking performance.

As an approach to developing long cavity lasers, we explored the use of Herriott style multiple pass cavity (MPC).[50] The MPC is constructed by a pair of curved mirrors separated by a given distance. The optical beam is introduced into the MPC, strikes the first mirror off center, is subsequently reflected between the two mirrors in a circular pattern, and can be extracted after a given number of round trips. The beam is also focused on subsequent reflections so that its propagation resembles propagation through a periodic lens array. This device is designed such that it provides a unity transformation of the q parameter of the laser beam after a given number of transits.[51] Thus, if this

---

44 MIT Lincoln Laboratories, Lexington, Massachusetts.

45 Professor, International Laser Center, Polytechnical Academy, Minsk, Belarus.

46 I.D. Jung, F.X. Kärtner, N. Matuschek, D.H. Sutter, F. Morier-Genoud, G. Zhang, and U. Keller, "Self-starting 6.5-fs Pulses from a Ti:sapphire Laser," *Opt. Lett.* 22: 1009-11 (1997).

47 H.A. Haus. J.G. Fujimoto, and E.P. Ippen, "Structures for Additive Pulse Modelocking," *J. Opt. Soc. Am. B* 8: 2068 (1991); H.A. Haus, J.G. Fujimoto, and E.P. Ippen, "Analytic Theory of Additive Pulse and Kerr Lens Mode Locking," *IEEE J. Quant. Electron* 28: 2086 (1992).

48 M. Ramaswamy, M. Ulman, J. Paye, and J.G. Fujimoto, "Cavity-dumped Femtosecond Kerr-lens Mode-locked Ti:Al_2O_3 Laser," *Opt. Lett.* 18: 1822-24 (1993).

49 L. Xu, G. Tempea, A. Poppe, M. Lenzner, C. Spielmann, F. Krausz, A. Stingl, and K. Ferencz, "High-power Sub-10-fs Ti:sapphire Oscillators," *Appl. Phys. B* 65: 151-59 (1997).

50 D. Herriott, H. Kogelnik, and R. Kompfner, "Off-Axis Paths in Spherical Mirror Interferometers," *Appl. Opt.* 3: 523-26 (1964); B. Perry, R.O. Brickman, A. Stein, E.B. Treacy, and P. Rabinowitz, "Controllable Pulse Compression in a Multiple-pass Raman Laser," *Opt. Lett.* 5:288 (1980).

51 H.A. Haus, *Waves and Fields in Optoelectronics* (Englewood Cliffs, New Jersey: Prentice-Hall, 1984), pp.128-38.

device is inserted into the KLM laser, it can be designed such that it has a zero effective length and leaves the laser cavity mode and nonlinear focusing behavior invariant.

Following this approach, we designed a high peak power laser using a standard, dispersion compensated KLM Ti:Al_2O_3 resonator with a MPC incorporated into one of the arms. We used a design for which the beam made 20 round trips between the MPC mirrors. Stable KLM modelocking was achieved resulting in 20 fs pulses at 15 MHz repetition rate, compared to a repetition rate of 100 MHz typical for conventional resonator geometries. This resulted in a higher peak power for a given average output power. Furthermore, because the pulse repetition rates are significantly lower, parasitic thermal effects in ultrafast measurements using this source will be significantly smaller than for conventional high repetition rate 100 MHz lasers.

A limitation on the available pulse energies in our system was imposed by multiple pulse instabilities that tend to arise at high-pulse energies. This is a consequence of the high-peak intensities present in this laser and the saturation of the self amplitude modulation effects. As the length of the laser cavity is increased, the intracavity pulse energies and intensities are also increased to higher levels than in standard lasers.

A detailed understanding of the KLM mechanism and the cavity operation is required for further improvement of the laser operation. We are currently optimizing the laser design in order to achieve shorter pulse duration and higher output power while avoiding multiple pulsing.

1.14.2 Novel Saturable Absorber Materials and Devices

Over the past several years, significant advances have been made in generation of ultrashort optical pulses from passively modelocked solid state lasers. Kerr-lens modelocking is the most widely used modelocking technique, but it is generally not self-starting and requires very precise resonator design and alignment. For starting and stabilization of modelocking, a fast saturable absorber with low losses and appropriate saturation intensity is required.

In recent years, there has been a large amount of work done in application of semiconductor saturable absorbers to laser modelocking.[52] Compared to other approaches to laser modelocking, saturable absorbers have a number of advantages, including self-starting operation, robustness and simplicity of laser design, and a number of adjustable parameters including operating wavelength, recovery time, and saturation fluence which make it possible to tailor the device parameters for a specific application. This powerful technology has been applied for both modelocking and self-starting in a wide range of laser materials in the 0.8, 1.0, 1.3, and 1.5 μm wavelengths regions.

Although this technology has significant advantages, it also has the major disadvantage of requiring epitaxial growth (typically molecular or chemical beam expitaxy) of semiconductor layers. Epitaxial materials growth is complex and costly and thus is a barrier to widespread commercial application of semiconductor saturable absorbers.

Semiconductor doped color glasses, which have high nonlinearities and rapid relaxation times, can potentially offer a simple and inexpensive alternative to semiconductor saturable absorber mirrors. In earlier studies, infrared color filter glass from Hoya (Hoya IR76) has been demonstrated to generate self-starting 2.7 ps pulses from a Ti:Al_2O_3 laser.[53]

We have designed novel modelocking devices based on commercial color filter glass for both saturable absorber and self-starting KLM operation in a Ti:Al_2O_3 laser. Commercial semiconductor doped color glasses from Schott (RG-850 and RG-780) were attached to silica or sapphire substrates and the structure was ground at an angle of 1 degree resulting in a wedge of color glass on top of the substrate. The wedge-shaped design enabled us to obtain thinner color glass than otherwise possible (down to 20 μm) and to continuously vary the saturable absorber loss by changing the color glass inser-

52 U. Keller, K.J. Weingarten, F.X. Kärtner, D. Kopf, B. Braun, I.D. Jung, R. Fluck, C. Hönninger, N. Matuschek, and J. Aus der Au, "Semiconductor Saturable Absorber Mirrors (SESAM's) for Femtosecond to Nanosecond Pulse Generation in Solid-State Lasers," *IEEE J. Select. Top. Quantum Electron.* 2: 435-53 (1996); S. Tsuda, W.H. Knox, S.T. Cundiff, W.Y. Jan, and J.E. Cunningham, "Mode-Locking Ultrafast Solid-State Lasers with Saturable Bragg Reflectors," *IEEE J. Select. Top. Quantum Electron.* 2: 454-64 (1996).

53 N. Sarukura, Y. Ishida, T. Yanagawa, and H. Nakano, "All Solid State CW Passively Mode-locked Ti:Sapphire Laser Using a Colored Glass Filter," *Appl. Phys. Lett.* 57: 229-30 (1990).

tion. The sapphire substrate made the structure more robust than previous designs using thin free standing glass and also served as an efficient heat sink, reducing parasitic thermal effects.

We used a standard z-shaped cavity terminated with an additional fold comprising two 10 cm radius of curvature mirrors. By placing the saturable absorber at or near the focus of the additional fold, we obtained self-starting saturable absorber modelocked operation with pulse durations of 1.9 ps. Varying the saturable absorber position relative to the focus enabled us to vary the effective saturation cross-section. Using a birefringent filter, tunable modelocked operation was achieved from 780 to 850 nm using RG-780 glass and from 840 to 870 nm using RG-850 glass.

Self-starting modelocked operation was also achieved using the RG-850 glass saturable absorber in conjunction with a resonator optimized for Kerr lens modelocking (KLM) resulting in self-starting 52 fs transform limited pulses. The self-starting KLM operation was robust and insensitive to cavity perturbations. An intracavity chopper was used to study the modelocking self-starting dynamics by monitoring both the average power and the second harmonic (SHG) signal. The modelocking build up time was measured to be 1.5 ms.

We believe that the spectrum, and therefore the ultimate pulse duration, is limited by the spectral filtering combination of the mirror set on the long wavelength side and the rapidly increasing absorption of the RG-850 glass on the short wavelength side. Using thinner glass structures or color glass with lower semiconductor doping density would greatly increase tunabilty to shorter wavelengths and support broader spectra, thus leading to shorter pulses. We are also currently working on incorporating the color glass saturable absorber into a reflective geometry dielectric mirror device which will further simplify the laser design.

We believe that devices incorporating commercial or experimental semiconductor doped color glasses can potentially serve as simple and inexpensive devices for both initiating KLM and modelocking solid-state lasers.

1.14.3 Rapid Wavelength Tuning of Near-IR Lasers

Rapid wavelength tuning of solid-state lasers is important for a number of applications including optical ranging, optical communications, Raman spectroscopy, and fluorescence spectroscopy. Earlier studies of frequency tunable sources used methods such as acousto-optic tuning[54] and thermal tuning[55] to scan the wavelength range.

In the past year, we have extended our previous research on the spectroscopy and modelocking of chromium-doped forsterite (Cr^{4+}:Mg_2SiO_4) lasers to develop a new rapidly tunable source in the near infrared. Cr^{4+}:forsterite has a 200 nm cw tuning range,[56] making it suitable for rapidly and broadly tunable laser. We implemented this laser using a standard z-cavity configuration. The wavelength selection, as well as spectral filtering, was accomplished by inserting four Brewster angled prisms and a cavity end-mirror into one arm of the cavity. The angular deflection of a light beam passing through the prisms is wavelength dependent, and therefore a narrow band of frequencies will be returned after reflecting from the end mirror; more prisms give stronger wavelength filtering. By tilting the end mirror, we tuned the frequencies emitted from the laser. This was done by placing the end-mirror upon a tilting galvanometer, which was driven with triangular voltage waveforms at frequencies up to 1 kHz and angular deflection amplitudes sufficient to cover the bandwidth of the laser. With this source, the tuning range of 1200 to 1275 nm can be swept in less than 500 μs. Scanning speeds are limited by cavity mode buildup times and relaxation oscillation effects. Cr:forsterite presents a broadband, relatively high power, and simple rapidly tunable laser source in the 1.3 μm wavelength region, important for optical communications.

54 K. Takada, "High-Resolution OFDR with Incorporated Fiber-Optic Frequency Encoder," *IEEE Photonics Technol. Lett.* 4: 1069-72 (1992)

55 U. Glombitza and E. Brinkmeyer, "Coherent Frequency-Domain Reflectometry for Characterization of Single-Mode Integrated Optical Waveguides," *J. Lightwave Technol.* 11: 1377-84 (1993)

56 B. Golubovic, *Study of Near-Infrared Pumped Solid-State Lasers and Applications*, Ph.D. diss., Department of Electrical Engineering and Computer Science, MIT, 1997.

In optical frequency domain reflectometry (OFDR), a cw laser is used as the input to an interferometer and is swept over a wide range of frequencies. A delay introduced into one arm of the interferometer causes a difference between the frequencies of the light which are returned from the two arms. This frequency difference can be detected by interfering the two beams and can then be used to determine the path-length difference between the arms of the interferometer. By utilizing a frequency-domain technique to tune the laser, we demonstrated OFDR and imaging at resolutions similar to those achieved using modelocked lasers and low-coherence interferometry. The frequency domain techniques can have the advantage of a significant reduction in system complexity and still achieve high resolution since the distance resolution of the system is proportional to the tuning bandwidth of the laser.

1.14.4 Optical Frequency Domain Reflectometry Using Rapid Wavelength Tuning

Optical ranging and tomographic techniques have applications to various fields from engineering to medicine. Optical frequency domain reflectometry (OFDR) is based on interferometry and allows for very high-resolution axial measurements compared to optical time domain reflectometry (OTDR).[57] Another attractive feature of OFDR is that ranging can be performed without the need for mechanical scanning of the path length of the interferometer reference arm like in optical coherence tomography (OCT),[58] and it scans the wavelength of a narrow-band source. Moreover, obtaining high single-transverse-mode power from a broadband light source may present technical difficulties; a tunable narrow-band source of equal brightness may be significantly less complex.

OFDR uses a fixed reference path and continuously sweeps a narrow-band optical source over a wide span of frequencies. In this case, the wavelength of the light detected at the interferometer output port is a function of time. Ranging is performed by means of a Michelson interferometer for which both arms are of fixed length, one terminated by a reference mirror, and the other by the sample under investigation. Introducing a relative temporal delay into this interferometer will then give rise to a difference in the wavelength of the light emitted from each arm. The frequency of the beat at the output port of the interferometer is then used to determine the pathlength difference and to localize backreflection sites in the sample arm. Previous studies of the use of tunable sources for OFDR were typically based on frequency-tunable semiconductor diode laser systems. In our system we present the use of a rapidly tuned cw Cr^{4+}:forsterite(Cr^{4+}:Mg_2SiO_4) laser[59] for OFDR applications.

This system achieves high resolution imaging utilizing the high power and broad bandwidth potential of solid-state lasers. A depth resolution of 15 μm was demonstrated, with speeds as fast as 2000 longitudinal scans per second. The signal-to-noise ratio of this system was measured to be 70 dB. Using other tunable solid-state laser materials, one could perform optical ranging and OCT with high resolution at other wavelengths at which ultrashort-pulse generation is problematic. The ultimate extension of these techniques using narrow-linewidth tunable diode laser sources would afford even higher scanning speeds and greater ease of use.

1.14.5 Publications

Bilinsky, I.P., B.E. Bouma, and J.G. Fujimoto. "Self-starting KLM Ti:Al_2O_3 Laser Using Semiconductor Doped Glass Structures." Paper presented at the 1998 Conference on Lasers And Electro-Optics, San Francisco, California, May 2-8, 1998.

Cho, S.H., B.E. Bouma, E.P. Ippen, and J.G. Fujimoto. "A 15 MHz High Peak Power KLM Ti:Al_2O_3 Laser using Multiple Pass Long Cavity." Paper presented at the 1998 Conference on Lasers And Electro-Optics, San Francisco, California, May 2-8, 1998.

Golubovic, G., B.E. Bouma, G.J. Tearney, and J.G. Fujimoto. "Optical Frequency-Domain Reflectometry using Rapid Wavelength Tuning of a

57 S.D. Personick, "Photon Probe Optical-fiber Time-domain Reflectometer," *Bell Syst. Tech. J.* 56: 355-66 (1977); D. Uttam and B. Culshaw, "Precision Time Domain Reflectometry in Optical Fiber Systems using a Frequency Modulated Continuous Wave Ranging Technique," *J. Lightwave Technol.* 3: 971-977 (1985).

58 D. Huang, E.A. Swanson, C.P. Lin, J.S. Schuman, W.G. Stinson, W. Chang, M.R. Hee, T. Flotte, K. Gregory, C.A. Puliafito, and J.G. Fujimoto, "Optical Coherence Tomography," *Sci.* 254: 1178-81 (1991).

59 B. Golubovic, B.E. Bouma, I.P. Bilinsky, J.G. Fujimoto, and V.P. Mikhailov, "Thin Crystal, Room-temperature Cr^{4+}:Forsterite Laser using Near-infrared Pumping," *Opt. Lett.* 21: 1993-95 (1996).

Cr^{4+}:Forsterite Laser." *Opt. Lett.* 22: 1704-06 (1997).

1.15 Laser Medicine and Medical Imaging

Sponsors

National Institutes of Health
Grant 9RO1 EY11289-12
Grant 1R01 CA75289-01
U.S. Air Force - Office of Scientific Research
Contract F49620-95-1-0221
U.S. Navy - Office of Naval Research/MFEL
Contract N00014-94-1-0717
Contract N000014-97-1-1066

Project Staff

Stephen A. Boppart, Dr. Brett E. Bouma, Dr. Mark E. Brezinski,[60] Michael R. Hee, Dr. Jürgen Herrmann,[61] Constantinos Pitris, Guillermo J. Tearney, Professor James G. Fujimoto, Eric A. Swanson,[62] Dr. Carmen Puliafito,[63] Dr. Joel Schuman[64]

1.15.1 Optical Coherence Tomography Technology

Optical coherence tomography (OCT) is a new imaging technology which was developed by our group in 1991.[65] OCT is analogous to ultrasound or radar imaging except that it uses light instead of sound to perform high resolution cross sectional imaging of biological specimens and materials. It allows *in vitro* or *in vivo* imaging of tissue in virtually any organ accessible via catheter or endoscope, generating two-dimensional tomographic images of tissue microstructure or three-dimensional reconstructed volumes.

OCT was first used to image optically transparent structures such as the anterior eye and retina.[66] Preliminary clinical investigations suggest that OCT is a promising technology for the detection and management of a variety of retinal diseases including glaucoma and macular edema.[67] Recent advances have led to the application of this modality to non-transparent tissue.[68] Although the imaging depth of OCT is limited by the light scattering and attenuation properties of tissue, penetration of 2-3 mm can be achieved even in heavily calcified samples. The resolution of OCT is on the micron scale, up to two orders of magnitude higher than conventional ultrasound. In essence, imaging is being performed over the distance of a conventional biopsy and near the resolution of histopathology, hence the description of OCT as an "optical biopsy." Previous studies with OCT have included the identification of pathology in the cardiovascular system, gastrointestinal tract, and skin, in addition to studies of normal urinary tract, nervous system, and reproductive tract.[69] A small catheter-endoscope system has also been developed which allowed high resolution imaging to be performed *in vivo* in a rabbit model.[70]

60 Research Affiliate, Cardiac Unit, Massachusetts General Hospital and Harvard Medical School, Boston, Massachusetts.

61 Visiting Scientist, University of Erlangen, Germany.

62 MIT Lincoln Laboratory, Lexington, Massachusetts.

63 Chairman, Department of Ophthalmology, New England Eye Center, Tufts University Medical School and Director, Boston, Massachusetts.

64 Director, Glaucoma Services, New England Eye Center, Tufts New England Medical Center, Boston, Massachusetts.

65 D. Huang, E.A. Swanson, C.P. Lin, J.S. Schuman, W.G. Stinson, W. Chang, M.R. Hee, T. Flotte, K. Gregory, C.A. Puliafito, J.G. Fujimoto, "Optical Coherence Tomography," *Sci.* 254: 1178-81 (1991).

66 M.R. Hee, J.A. Izatt, E.A. Swanson, D. Huang, C.P. Lin, J.S. Schuman, C.A. Puliafito, and J.G. Fujimoto, "Optical Coherence Tomography of the Human Retina," *Arch. Ophthalmol.* 113: 325-32 (1995); E.A. Swanson, J.A. Izatt, M.R. Hee, D. Huang, C.P. Lin, J.S. Schuman, C.A. Puliafito, and J.G. Fujimoto, "*In Vivo* Retinal Imaging by Optical Coherence Tomography," *Opt. Lett.* 18: 1864-66 (1993).

67 C.A. Puliafito, M.R. Hee, C.P. Lin, E. Reichel, J.S. Schuman, J.S. Duker, J.A. Izatt, E.A. Swanson, and J.G. Fujimoto, "Imaging of Macular Diseases with Optical Coherence Tomography," *Ophthalmol.* 102: 217-29 (1995).

68 C.A. Puliafito, M.R. Hee, J.S. Schumann, and J.G. Fujimoto, "Optical Coherence Tomography of Ocular Diseases," (Thorofare, New Jersey: SLACK Incorporated, 1995); J.G. Fujimoto, M.E. Brezinski, G.J. Tearney, S.A. Boppart, B.E. Bouma, M.R. Hee, J.F. Southern, and E.A. Swanson, "Optical Biopsy and Imaging Using Optical Coherence Tomography," *Nature Med.* 1: 970-72 (1995); J. Schmitt, M. Yadlowsky, and R. Bonner, "Subsurface Imaging of Living Skin with Optical Coherence Microscopy," *Dermatol.* 191: 93-98 (1995).

69 M.E. Brezinski, G.J. Tearney, B.E. Bouma, J.A. Izatt, M.R. Hee, E.A. Swanson, J.F. Southern, and J.G. Fujimoto, "Optical Coherence Tomography for Optical Biopsy. Properties and Demonstration of Vascular Pathology," *Circulat.* 93(6): 1206-13 (1996).

70 Y. Pan, E. Lankenau, J. Wlezel, R. Birngruber, and R. Engelhardt, "Optical Coherence-gated Imaging of Biological Tissues," *Sel. Topics Quantum Electron.* 2: 1029-34 (1996); J.A. Izatt, M.D. Kulkarni, H.W. Wang, K. Kobayashi, and M.V. Sivak, "Optical Coherence Tomography and Microscopy in Gastrointestinal Tissues," *Sel. Topics Quantum Electron.* 2: 1017-28 (1996).

OCT is based on the detection of infrared light waves that are back-scattered or reflected from different layers and structures within the tissue. Utilizing a Michelson interferometer, the beam leaving the optical light source is split into two parts, a reference and a sample beam. The reference beam is reflected off of a mirror at a known distance and returns to the detector. The sample beam reflects off of different layers within the tissue. Light returning from the sample and reference arms recombines and if the two light beams have traveled the same distance (optical pathlength), the two beams will interfere. Low coherence can be used to localize backreflection sites and provide the desired high axial resolution. OCT measures the intensity of the interference obtained from different points within the tissue by moving the mirror in the reference arm which changes the distance light travels in that arm. Two or three dimensional images are produced by scanning the beam across the sample and recording the optical backscattering versus depth at different transverse positions. The resulting data is a two or three dimensional representation of the optical backscattering of the sample on a micron scale.

With previous OCT systems, the optical delay in the reference arm was varied with either a linearly translating galvanometer or by stretching an optical fiber with a piezoelectric crystal.[71] However, commercial galvanometers do not generate sufficient mechanical translation rates to allow imaging in real time. Piezoelectric fiber stretchers allow rapid scanning, but they suffer from high power requirements, nonlinear fringe modulation due to hysteresis, uncompensated polarization dispersion matches, and poor temperature stability. For these reasons, we designed a high-speed optical delay line using phase control techniques originally developed for femtosecond pulse shaping.[72] This device can be constructed with common optical components, has modest power requirements, is repeatable, and is temperature stable.[73] The phase control optical delay line contained a lens-grating pair to Fourier transform the temporal profile of the low-coherence (broad-spectrum) light in the reference arm. A mirror, mounted to a galvanometer, placed at the Fourier plane, allowed angular tilt to be mapped to group delay.[74] The group delay was varied by rapidly changing the angle of the mirror mounted to the galvanometer, allowing the acquisition of 2000 axial scans per second, or 4 to 8 frames per second, with a total optical path length delay of ~3 mm. This method, in conjunction with a fiber optic catheter/endoscope was used to perform *in vivo* OCT imaging for the first time.[75]

The delivery of optical radiation for medical diagnostic and imaging applications has motivated several unique optical system designs. Forward-imaging devices overcome a limitation of side-imaging devices; permitting data to be collected before introducing the device into tissue. This concept also permits the image-guided placement of the device in surgery and for monitoring interventional procedures such as tissue incision, resection, and laser surgery. To perform forward-imaging of a single-mode beam, a lens, fiber, or combination thereof may be translated with motors, piezoelectric cantilevers, or electrostatic/magnetic techniques.

A second design permits variable magnification by scanning a cleaved fiber tip in the focal plane of the first lens in a telescope. The beam is collimated and then focused by a second lens which effectively relay-images the fiber tip onto the object or specimen. The advantages of this design include low mass on the piezoelectric cantilever permitting higher translation velocities and interchangeable magnification via different lenses.[76] In contrast to the hand-held

71 V.M. Gelikonov, G.V. Gelikonov, R.V. Kuranov, K.I. Pravdenko, A.M. Sergeev, F.I. Feldshtein, Y. I. Khanin, D.V. Shabanov, N.D. Gladkova, N.K. Nikulin, G.A. Petrova, and V.V. Pochinko, "Coherent Optical Tomography of Microscopic Inhomogeneities in Biological Tissues," *JETP Lett.* 61(2): 158-62 (1995); G.J. Tearney, B.E. Bouma, S.A. Boppart, B. Golubovic, E.A. Swanson, and J.G. Fujimoto, "Rapid Acquisition of *In Vivo* Biological Images by use of Optical Coherence Tomography," *Opt. Lett.* 21(17): 1408-10 (1996).

72 K.F. Kwong, D. Yankelevich, K.C. Chu, J.P. Heritage, and A. Dienes, "400-Hz Mechanical Scanning Optical Delay Line," *Opt. Lett.* 18(7): 558-60 (1993); J.A. Izatt, M.D. Kulkarni, H.W. Wang, K. Kobayashi, and M.V. Sivak, "Optical Coherence Tomography and Microscopy in Gastrointestinal Tissues," *Sel. Topics Quantum Electron.* 2: 1017-28 (1996).

73 G.J. Tearney, B.E. Bouma, and J.G. Fujimoto, "High Speed, Phase- and Group-delay Scanning with a Grating-based Phase Control Delay Line," *Opt. Lett.* 22: 1811-13 (1997).

74 R.P. Salathe, H. Gilgen, and G. Bodmer, "Coupled-mode Propagation in Multicore Fibers Characterized by Optical Low-coherence Reflectometry," *Opt. Lett.* 21(13): 1006 (1996).

75 G.J. Tearney, M.E. Brezinski, B.E. Bouma, and S.A. Boppart, C. Pitris, J.F. Southern, and J.G. Fujimoto, "*In Vivo* Endoscopic Optical Biopsy with Optical Coherence Tomography," *Sci.* 276: 2037-39 (1997).

76 S.A. Boppart, B.E. Bouma, C. Pitris, G.J. Tearney, and J.G. Fujimoto, "Forward-scanning Instruments for Optical Coherence Tomographic Imaging," *Opt. Lett.* 22: 1618-20 (1997).

probe for open-field surgical procedures, rigid laparoscopes permit visualization of tissue at distant (10-50 cm) internal sites while maintaining a small instrument diameter for insertion through small incisions during minimally invasive surgical procedures. A single rod lens or a series of relay lenses (Hopkins-type) can be used to image.[77] The laparoscope also permits simultaneous en face OCT imaging of the area. A rigid OCT laparoscope was constructed using a 2.68 mm diameter, 19.5 cm long, rod lens with a nominal pitch length of 3/2 for visible wavelengths. To demonstrate the imaging capability of the hand-held probe design, *in vitro* images of human ovary and lung were acquired with 12 μm axial and 31 μm transverse resolution. The external surface imaging orientation for the ovary is similar to that encountered during open-field surgical procedures. In summary, we have presented hand-held probe and rigid laparoscope forward-imaging optical instruments for optical coherence tomographic imaging. These two devices represent different approaches for OCT imaging and can be powerful diagnostic tools for medical and surgical applications. In future applications, OCT imaging might also be integrated with laser-based surgery to permit the simultaneous visualization and surgical incision of tissues on a micron scale.

1.15.2 Optical Biopsy Using Optical Coherence Tomography

A technology capable of performing optical biopsy should prove to be a powerful diagnostic modality in clinical medicine. Optical biopsy is defined here as imaging tissue microstructure at or near the level of histopathology without the need for tissue excision. At least three clinical scenarios exist in which optical biopsy will likely have a considerable impact on patient management. The first is in situations in which sampling errors severely restrict the effectiveness of excisional biopsy, such as the high failure rates associated with blind biopsies used to screen the premalignant conditions of ulcerative colitis or Barrett's esophagus.[78] A need also exists for optical biopsy when conventional excisional biopsy is potentially hazardous. Examples of vulnerable regions include the central nervous system, the vascular system, and articular cartilage. Finally, the ability to image at the cellular level could improve the effectiveness of many surgical and microsurgical procedures including coronary atherectomy, transurethral prostatectomies, and microvascular repair.[79]

Myocardial infarction, better known as a heart attack, remains one of the most commonly diagnosed problems in hospitalized patients in the United States. Most heart attacks are caused by the rupture of an atherosclerotic plaque, which results in thrombus formation and subsequent coronary artery occlusion. Plaques exhibiting large lipid cores held by weak fibrous caps are at the greatest risk of rupture. Currently, imaging modalities such as angioscopy, ultrasound, and MRI are not able to identify these high-risk plaques. Angioscopy is limited because only the surface of the artery can be viewed in the absence of blood. Ultrasound and MRI are both limited by low resolution and dynamic range. In addition, MRI is an expensive and complicated diagnostic tool. OCT's high resolution enabled a series of *in vitro* experiments to examine arterial structure including intimal wall thickness, lipid content, and even heavily calcified plaques.[80] Following the development of a catheter-based OCT system, an *in vitro* study comparing the resolution of OCT and intravascular ultrasound was performed. The images obtained using OCT yielded superior structural detail in all plaques examined.[81] OCT's fiber optic design has the ability to be delivered through intravascular catheters, making clinical diagnosis and surgical guidance practical

77 T.H. Tomkinson, J.L. Bently, M.K. Crawford, C.J. Harkrider, D.T. Moore, and J.L. Rouke, "Rigid Endoscopic Relay Systems: A Comparative Study," *Appl. Opt.* 35(34): 6674-83 (1996).

78 R.W. Phillips and R.K.H. Wong, "Barret's Esophagus. Natural History, Incidence, Etiology, and Complications," *Gastroenterol. Clin. N. Am.* 20: 791 (1991).

79 G.J. Tearney, M.E. Brezinski, J.F. Southern, B.E. Bouma, S.A. Boppart, and J.G. Fujimoto, "Optical Biopsy in Human Urologic Tissue Using Optical Coherence Tomography," *J. Urol.* 157: 1915-19 (1997); M.E. Brezinski, G.J. Tearney, S.A. Boppart, E. A. Swanson, J.F. Southern, and J.G. Fujimoto, "Optical Biopsy with Optical Coherence Tomography: Feasibility for Surgical Diagnostics," *J. Surgical Res.* 71(1): 32-40 (1997).

80 M.E. Brezinski, G.J. Tearney, B.E. Bouma, S.A. Boppart, M.R. Hee, E.A. Swanson, J.F. Southern, J.G. Fujimoto, "Imaging of Coronary Artery Microstructure (*In Vitro*) with Optical Coherence Tomography," *Am. J. Cardiol.* 77: (1996).

81 G.J. Tearney, M.E. Brezinski, S.A. Boppart, B.E. Bouma, N. Weissman, J.F. Southern, E.A. Swanson, and J.G. Fujimoto, "Catheter-based Optical Imaging of a Human Coronary Artery," *Circulat.* 94: 3013 (1996); M.E. Brezinski, G.J. Tearney, N.J. Weissman, S.A. Boppart, B.E. Bouma, M.R. Hee, A.E. Weyman, E.A. Swanson, J.F. Southern, and J.G. Fujimoto, "Assessing Atherosclerotic Plaque Morphology: Comparison of Optical Coherence Tomography and High Frequency Intravascular Ultrasound," *Brit. Heart J.* 77: 397-403 (1997).

applications of this technology. The ability to detect small atherosclerotic plaques as well as existing fissures in the vessel long before they rupture has obvious benefits in heart attack prevention.

Cancer is second only to heart disease as a leading cause of mortality in the industrialized world.[82] Effective screening and detection of early neoplastic changes are important in improving a patient's prognosis, since once metastatic, treatment is difficult while cure, for the most part, is not possible.[83] Many existing diagnostic modalities, including x-ray imaging, ultrasound, and endoscopy do not have sufficient resolution to detect changes associated with early neoplasia. Excisional biopsy, which is the gold standard for diagnosis, is based mostly on the identification of structural and cellular changes associated with the disease. Excision of specimens, however, is sometimes not possible, has limited area coverage, and can lead to unacceptable false negative rates because of sampling errors.[84] Interventional decisions require accurate diagnosis and positive identification of the tumor margins which are not easily and readily quantifiable due to the limitations associated with conventional biopsies.

A diagnostic imaging technology that can perform real-time, high resolution tomographic imaging of the architectural morphology of tissue in situ could improve the diagnosis of early neoplasia and thus reduce morbidity and mortality. Optical coherence tomography cold fill this void. OCT imaging was performed *in vitro* on a series of human tissues of varying degrees of neoplastic infiltration, including colon, cervix, uterus and lung. Microstructural and epithelial changes associated with neoplasia, such as dilated and distorted glands, were readily imaged and favorably matched to histopathology. We were also able to investigate the structure and organization of the epithelium and assess where it was destroyed and the integrity of the basal membrane was compromised. In more advanced stages of cancer, neo-vascularization was also evident.

Although the penetration of OCT imaging is limited to a few millimeters, it is sufficient to image epithelial cell layers in most organ systems and detect changes associated with early neoplasia. OCT features, described earlier, coupled with the recent experimental results suggest that OCT could provide an effective tool for the diagnosis and assessment of neoplastic changes of tissue.[85]

1.15.3 In-Vivo Imaging with Optical Coherence Tomography

A major step in promoting OCT as a clinically viable and diagnostically useful imaging modality, is investigating and assessing its capabilities *in vivo*. To do so, we have demonstrated *in vivo* endoscope-based OCT imaging of the gastrointestinal, respiratory and cardiovascular tracts in an animal model with an axial resolution of 10 mm at four to eight frames per second. The optical delay line and catheter/endoscope, both described earlier, were used to image normal, 12-week-old New Zealand White rabbits.

OCT images of the *in vivo* rabbit esophagus allowed visualization of all layers of the esophageal wall. For example, the innermost layer, the mucosa, was readily distinguished owing to its low reflectivity compared with the submucosa. Vascular structures were also identified within the wall. These high-resolution images demonstrate the capability of OCT to both resolve micro-structural detail and image the entire rabbit esophagus to the serosa. *In vivo* OCT images of the rabbit trachea permitted differentiation of the pseudostratified epithelium, mucosa, and surrounding hyaline cartilage. Because most neoplasms of the esophagus and respiratory tract originate in the epithelium, the ability of OCT to precisely identify the mucosa could have important clinical implications.

In vivo OCT imaging (Figure 17) of a living rabbit's aorta was performed via a small, catheter-based system with a 10 μm resolution. OCT's intravascular imaging represented a ten fold improvement in resolution over "state of the art" intravascular ultrasound (IVUS) transducers. High contrast was noted

82 S.L. Parker, T. Tong, S. Bolden, and P.A. Wingo, "Cancer Statistics 1997," *CA* 47(1): 5-27 (1997).

83 R.T. Osteen, ed., *Cancer Manual*, 8th ed. (Boston: American Cancer Society, 1990).

84 K.W. Wang and E.P. DiMagno, "Endoscopic Ultrasonography: High Technology and Cost Containment," *Gastroenterol.* 105(1): 283-86 (1993).

85 G.J. Tearney, S.A. Boppart, B.E. Bouma, M.E. Brezinski, N.J. Weissman, J.F. Southern, and J.G. Fujimoto, "Scanning Single-Mode Fiber Optic Catheter-Endoscope for Optical Coherence Tomography," *Opt. Lett.* 21(7): 543-45 (1996); M.E. Brezinski, G.J. Tearney, B.E. Bouma, J.A. Izatt, M.R. Hee, E.A. Swanson, J.F. Southern, and J.G. Fujimoto, "Optical Coherence Tomography for Optical Biopsy. Properties and Demonstration of Vascular Pathology," *Circulat.* 93(6): 1206-13 (1996).

between the media and the surrounding supportive tissue. In addition, fine structural detail was noted within the surrounding supportive tissue. This work, taken together with previous studies examining *in vitro* atherosclerotic plaque, strongly suggest a role for OCT in high-resolution intraarterial assessments of coronary atherosclerosis. An observation of particular importance in this study was the attenuation which resulted from the presence of blood. No significant structural information was obtained unless simultaneous injections of saline, at a relatively low pressure and small volumes, were performed. This likely results from the large numbers of scattering particles (i.e., RBCs) present within blood.[86] If saline injections are required for *in vivo* patient imaging, clinicians will need to weigh the increased resolution and low cost against the likely increase in procedure time. In this work, imaging of atherosclerotic samples was not performed. Future technology development will focus on increasing data acquisition rates and integrating the system with low cost light sources.

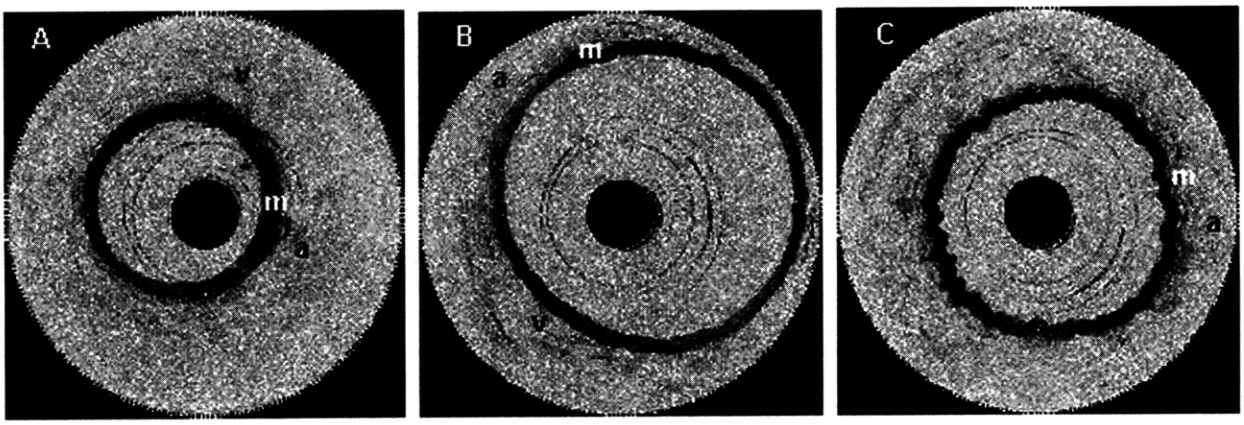

Figure 17. Rabbit aorta images after saline injection. Initiation of injection (A), maximal distention (B) and relaxation (C). Also visible are the media (m) and adventia (a) and a vein adjacent to the aorta (v).

1.15.4 Guiding Microsurgical Intervention with Optical Coherence Tomography

Optical instruments have become well-integrated into the surgical setting to visualize tissue and improve patient outcome. Surgical microscopes and loupes magnify tissue to prevent iatrogenic injury and to guide delicate surgical techniques. Although the repair of sensitive structures are performed with the aid of surgical microscopes to magnify the surgical field, surgeons have been limited to the *en face* view that they provide. OCT provides a technique capable of subsurface, three-dimensional, micron-scale imaging in real-time. This permits the intraoperative monitoring of microsurgical procedures, offering immediate feedback to the surgeon. Studies of *in vitro* surgical tissue specimens have shown potential for surgical diagnostics within the surgical operating suite.[87]

OCT is an optical imaging technology ideally suited for rapidly acquiring micron-scale resolution two- and three-dimensional images of biological tissue, such as small vessels and nerves. The OCT technology can be readily integrated with medical and surgical optical instruments. OCT imaging has been performed with a radial imaging flexible catheter/endoscope for accessing tortuous body lumens such as the gastrointestinal tract and vascular system.[88] A hand-held surgical probe has been developed for open-field surgical imaging and an OCT laparoscope has been constructed for internal imaging during

86 J.M. Steinke and A.P. Shepherd, "Comparison of Mie Theory and the Light Scattering of Red Blood Cells," *Appl. Opt.* 27: 4027-33 (1988).

87 M.E. Brezinski, G.J. Tearney, S.A. Boppart, E.A. Swanson, J.F. Southern, and J.G. Fujimoto, "Optical Biopsy with Optical Coherence Tomography, Feasibility for Surgical Diagnostics," *J. Surg. Res.* 71: 32-40 (1997).

88 G.J. Tearney, S.A. Boppart, B.E. Bouma, M.E. Brezinski, N.J. Weissman, J.F. Southern, and J.G. Fujimoto, "Scanning Single-mode Fiber Optic Catheter-endoscope for Optical Coherence Tomography," *Opt. Lett.* 21: 543-45 (1996).

minimally invasive surgical procedures.[89] OCT can function as a type of "optical biopsy," permitting the imaging of *in vivo* biological morphology without the need to excisionally remove and process a tissue specimen as in conventional histology.

Microsurgical procedures involve the re-anastomosis or re-attachment of severed nerves and vessels. These delicate operations are necessary to restore nerve function or vascular perfusion on the extremities or face following traumatic injury. To guide microsurgical interventions, the OCT technology was integrated with a stereo surgical microscope. The microscope enabled the location of the OCT imaging beam to be observed with high precision for real-time imaging during microsurgical procedures.[90] Arterial lumen obstruction is a leading cause of failure following microsurgical procedures. Cross-sectional OCT imaging enables immediate feedback to the operator and was used to locate intraluminal obstructions and potential thrombus-forming sites following the *in vitro* anastomosis of a severed artery. Identifying potential obstructions intraoperatively may improve the outcome of surgical procedures. In particular, identifying possible thromobogenic sites may reduce the incidence of late vascular occlusion after the injury site has been closed and bandaged.

OCT has also been used to image peripheral nerve fascicles in two and three dimensions. A peripheral nerve is composed of several smaller fascicle bundles. During surgical repair, corresponding fascicles from severed ends must be appropriately connected to effectively restore distal function. The three-dimensional imaging capabilities of OCT have been applied to tracking individual nerve fascicles along the axis of peripheral nerves. A 3D image with a segmented fascicle is shown in Figure 18. Also shown in this figure is a bifurcation of one fascicle which was not evident from 2D images. The use of OCT to intraoperatively assess microsurgical repair and to avoid subsurface vessels and nerves prior to incision offers promise for reducing patient morbidity and mortality following surgical procedures.

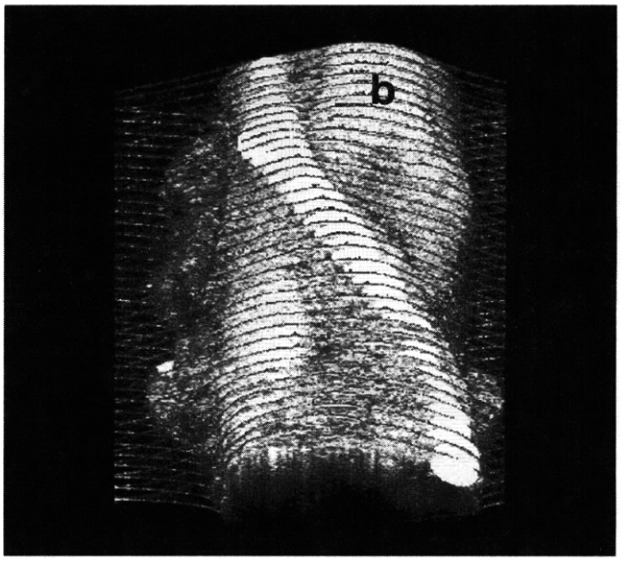

Figure 18. Three-dimensional OCT demonstrating individual fascicles within a human peripheral nerve. A bifurcation (b) observed in 3D was not apparent from 2D images.

1.15.5 Ophthalmic Imaging and Diagnosis with Optical Coherence Tomography

Strong collaborative efforts have led to the development and clinical application of an ophthalmic imaging OCT system. Working with MIT Lincoln Laboratory, a compact OCT system utilizing a fiber-coupled super-luminescent diode light source operating at 840 nm was integrated with a clinical ophthalmic slit-lamp biomicroscope. The biomicroscope permitted the operator to simultaneously visualize a patient's retina while viewing the position of the OCT imaging beam on the retina via a coincident visible aiming beam. The fully computer-controlled OCT system allowed arbitrary scan patterns on the retina or anterior eye structures.[91] Automated image processing routines have been developed to determine retinal thickness and produce multi-color topographic maps for rapid clinical assessment of ocular pathologies.

89 S.A. Boppart, B.E. Bouma, C. Pitris, G.J. Tearney, M.E. Brezinski, and J.G. Fujimoto, "Forward-imaging Instruments for Optical Coherence Tomographic Imaging," *Opt. Lett.* 22: 1618-20 (1997).

90 S.A. Boppart, B.E. Bouma, C. Pitris, G.J. Tearney, J.F. Southern, M.E. Brezinski, and J.G. Fujimoto, "Three-dimensional Optical Coherence Tomography for Microsurgical Diagnostics," *Radiol.*, forthcoming.

91 M.R. Hee, J.A. Izatt, E.A. Swanson, D. Huang, J.S. Schuman, C.P. Lin, C.A. Puliafito, and J.G. Fujimoto, "Optical Coherence Tomography of the Human Retina," *Arch. Ophthalmol.* 113: 325-32 (1995).

To date, ophthalmology has been the major clinical application for OCT. In collaboration with the New England Eye Center of Tufts University School of Medicine, over 5000 patients with a variety of macular diseases and diseases of the optic nerve head have been assessed and followed.[92] The technology has been transferred to industry and was introduced for clinical and research use in 1996 by Humphrey Instruments, a Division of Carl Zeiss, Inc. Approximately 100 units have been fielded to date. In many cases, OCT serves as the definitive diagnostic tool because it provides a cross-sectional image of retinal structure in addition to the surface features seen on fundoscopic exam. The cross-sectional view of OCT has been effective in the diagnosis and monitoring of macular holes, macular edema, retinal detachments,[93] macular degeneration,[94] and glaucoma.

The formation of macular holes is a retinal disease which often progresses to complete loss of central vision. OCT is useful for identifying early macular hole formation, staging macular hole progression, and for determining when surgical intervention is necessary.[95] Early surgical intervention can often prevent or correct vision loss. Macular edema is a disease where intraretinal fluid accumulation produces swelling and injury to the retina. The development of macular edema is a major treatable cause of vision loss in patient with diabetes. OCT is a more sensitive and objective indicator of retinal thickening due to macular edema than either slit-lamp biomicroscopy or fluorescein angiography. OCT can also quantitatively follow the resolution of edema following therapy. A topographic display protocol of macular thickness has been developed. The use of a standardized protocol means that OCT may have a significant impact on public health as a screening tool for the development of retinopathy in diabetic patients.

Recent efforts in the clinical application of OCT in ophthalmology have focused on the early diagnosis of glaucoma. Glaucoma is the third leading cause of blindness in the United States. Current diagnostic techniques such as direct and indirect ophthalmoscopy and evaluation of the cup-to-disc ratio are subjective. Measuring peripheral field loss in glaucoma patients provides quantitative parameters; however, up to 50% of the retinal nerve fiber layer may be lost prior to any noticeable symptoms. High-resolution cross-sectional OCT images of the retina permit reproducible nerve fiber layer thickness measurements within 10 to 20 microns.[96] Nerve fiber layer thickness measured by OCT correlates well with the functional status of the optic nerve and the visual field loss determined by traditional examination. Novel computer algorithms have been implemented to further improve the accuracy and monitoring of changes in nerve fiber layer thickness.[97] These results indicate that OCT is potentially able to detect the early onset of glaucoma before irreversible vision loss occurs.

1.15.6 Subcellular Optical Coherence Tomography Imaging: Implications for the Early Detection of Neoplasms

OCT is an optical imaging technology capable of subcellular resolutions which may ultimately have a role in the early diagnosis of malignancies. Neoplasias are most responsive to medical intervention at early stages, prior to undergoing metastasis. When these disorders arise from known premalignant states, and if a detection method exists, the high risk population can be screened to reduce patient morbidity and mortality. Organs where these premalignant conditions occur at relatively high frequency include the esophagus, uterus, bladder, colon, and

92 C.A. Puliafito, M.R. Hee, C.P. Lin, E. Reichel, J.S. Schuman, J.S. Duker, J.A. Izatt, E.A. Swanson, and J.G. Fujimoto, "Imaging of Macular Diseases with Optical Coherence Tomography," *Ophthalmol.* 102: 217-29 (1995).

93 M.R. Hee, C.A. Puliafito, C. Wong, E. Reichel, J.S. Duker, J.S. Schuman, E.A. Swanson, and J.G. Fujimoto, "Optical Coherence Tomography of Central Serous Chorioretinopathy," *Am. J. Ophthalmol.* 120: 65-74 (1995).

94 M.R. Hee, C.R. Baumal, C.A. Puliafito, J.S. Duker, E. Reichel, J.R. Wilkins, J.G. Coker, J.S. Schuman, E.A. Swanson, and J.G. Fujimoto, "Optical Coherence Tomography of Age-Related Macular Degeneration and Choroidal Neovascularization," *Ophthalmol.* 103: 1260-70 (1996).

95 M.R. Hee, C.A. Puliafito, C. Wong, J.S. Duker, E. Reichel, J.S. Schuman, E.A. Swanson, and J.G. Fujimoto," Optical Coherence Tomography of Macular Holes," *Opthalmol.* 102: 748-56 (1995).

96 J.S. Schuman, T. Pedut-Kloizman, E. Hertzmark, M.R. Hee, J.R. Wilkins, J.G. Coker, C.A. Puliafito, J.G. Fujimoto, and E.A. Swanson, "Reproducibility of Nerve Fiber Layer Thickness Measurements using Optical Coherence Tomography," *Ophthalmol.* 103: 1889-98 (1996).

97 D. Huang, M.R. Hee, L. Pieroth, T. Pedut-Kloizman, J.G. Coker, J.R. Wilkins, J.G. Fujimoto, E.A. Swanson, C.A. Puliafito, and J.S. Schuman, "A New Algorithm for Detecting Glaucomatous Nerve Fiber Layer Loss using Optical Coherence Tomography," Submitted to *Ophthalmol.*

stomach. The ability to image these organs in real-time at subcellular resolutions could represent a powerful tool for the early identification of neoplasms.

New technologies which have been pursued, with limited success, for the high-resolution assessment of subcellular structure include magnetic resonance imaging (MRI), x-ray microscopy, and high frequency ultrasound. These techniques, however, suffer from long acquisition times, potentially hazardous ionizing radiation, and direct contact with tissue, respectively. Recent advances in high-speed, *in vivo,* laser-scanning confocal microscopy have provided researchers with a means of imaging cellular morphology in skin.[98] However, confocal microscopy has a penetration depth limited to a few hundred microns and cannot be readily performed through an endoscope.

OCT combines the high resolutions of most optical techniques with an ability to reject multiply scattered photons and hence image at cellular resolutions up to millimeters deep in non-transparent tissue. Penetration limitations of other optical technologies are overcome by the use of near-infrared wavelengths which are absorbed and scattered less than shorter, visible wavelengths. Because OCT relies on variations in index of refraction and optical scattering for image contrast, no exogenous fluorophores are necessary for imaging which can limit the viability of living cells. OCT has been demonstrated as a useful research microscopy technique for developmental biology. *In vivo* developing embryos can be followed to observe the morphological expression of genes and genetic abnormalities.[99] High-speed OCT imaging has permitted the *in vivo* assessment of functional cardiovascular parameters in developing specimens.[100]

Although previous studies have demonstrated *in vivo* OCT imaging of tissue morphology, most have imaged tissue at resolutions of ~10-15 μm, which does not allow differentiation of cellular structure. The *Xenopus laevis* (African frog) tadpole, a common developmental biology animal model, was used to demonstrate the feasibility of OCT for *in vivo* subcellular imaging. A broad spectral bandwidth Kerr-lens modelocked Cr^{4+}:forsterite laser enabled resolution as high as 5 μm. OCT was able to identify the mitotic activity, the nuclear-to-cytoplasmic ratio, and the migration of developing cells for extended periods of time.[101] OCT images of cell structures were highly correlated with corresponding histology. A cross-sectional OCT image of actively dividing cells is shown in Figure 19. Individual cells, cell membranes, and cell nuclei are readily observed deep within the scattering tissue of a non-transparent tadpole. Melanin-laden neural crest cells are also observed along with the large hemisphere of the neural tube (brain). Three-dimensional neural crest cell migration has been followed in these specimens. These results have implications for OCT imaging of *in vivo* cellular morphology which, on extension to humans, could represent a powerful tool for the early evaluation of neoplastic changes.

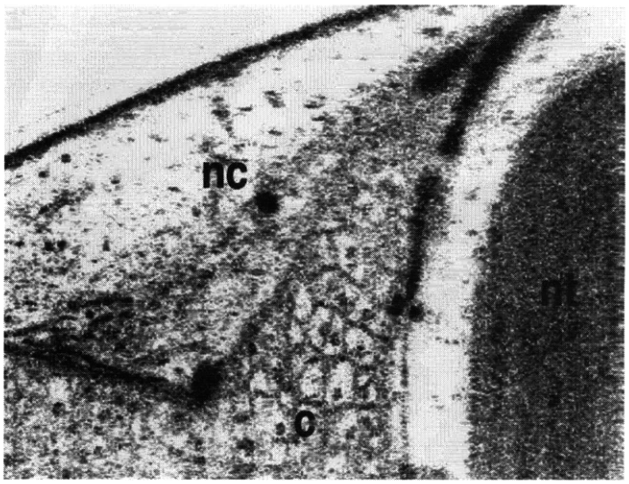

Figure 19. Subcellular OCT imaging within a developing *Xenopus* tadpole. Mitotically active cells (c) and migrating neural crest cells (nc) are observed *in vivo* next to the neural tube (nt) or brain of the tadpole.

98 M. Rajadhyaksha, M. Grossman, D. Esterowitz, R.H. Webb, and R.R. Anderson, "*In vivo* Confocal Scanning Laser Microscopy of Human Skin: Melanin Provides Strong Contrast," *J. Invest. Dermatol.* 104: 946-52 (1995).

99 S.A. Boppart, M.E. Brezinski, B.E. Bouma, G.J. Tearney, and J.G. Fujimoto, "Investigation of Developing Embryonic Morphology using Optical Coherence Tomography," *Dev. Biol.* 177: 54-64 (1996); S.A. Boppart, M.E. Brezinski, G.J. Tearney, B.E. Bouma, and J.G. Fujimoto, "Imaging Developing Neural Morphology using Optical Coherence Tomography," *J. Neurosci. Meth.* 70: 65-72 (1996).

100 S.A. Boppart, G.J. Tearney, B.E. Bouma, M.E. Brezinski, J.F. Southern, and J.G. Fujimoto, "Noninvasive Assessment of the Developing Xenopus Cardiovascular System using Optical Coherence Tomography," *Proc. Nat. Acad. Sci.* 94: 4256-61 (1997).

101 S.A. Boppart, B.E. Bouma, C. Pitris, J.F. Southern, M.E. Brezinski, and J.G. Fujimoto, "*In Vivo* Subcellular Optical Coherence Tomography Imaging in Xenopus laevis: Implications for the Early Diagnosis of Neoplasms," submitted to *J. Clinical Investigat.*

Publications

Boppart, S.A., B.E. Bouma, C. Pitris, G.J. Tearney, J.F. Southern, M.E. Brezinski, and J.G. Fujimoto. "Three-dimensional Optical Coherence Tomography for Microsurgical Diagnostics." *Radiol.* Forthcoming.

Boppart, S.A., M.E. Brezinski, C. Pitris, and J.G. Fujimoto. "Optical Coherence Tomography for the Identification of Human Brain Tumors and Margins." Submitted to *Neurosurg.*

Boppart, S.A., G.J. Tearney, B.E. Bouma, J.F. Southern, M.E. Brezinski, and J.G. Fujimoto. "Noninvasive Assessment of the Developing Xenopus Cardiovascular System using Optical Coherence Tomography." *Proc. Nat. Acad. Sci.* 94: 4256-61 (1997).

Boppart, S.A., B.E. Bouma, C. Pitris, G.J. Tearney, and J.G. Fujimoto. "Forward-scanning Instruments for Optical Coherence Tomographic Imaging." *Opt. Lett.* 22: 1618-20 (1997).

Boppart, S.A., B.E. Bouma, C. Pitris, J.F. Southern, M.E. Brezinski, J.G. Fujimoto. "*In Vivo*, High Speed Subcellular Imaging: Feasibility for the Early Diagnosis of Neoplasms." Submitted to *Nature Med.*

Bouma, B.E., L.E. Nelson, G.J. Tearney, D.J. Jones, M.E. Brezinski, and J.G. Fujimoto. "Optical Coherence Tomographic Imaging of Human Tissue at 1.55 mm and 1.8 mm using Er- and Tm-doped Fiber Sources." *J. Biomed. Opt.* Forthcoming.

Brezinski, M.E., G.J. Tearney, N.J. Weissman, S.A. Boppart, B.E. Bouma, M.R. Hee, A.E. Weyman, E.A. Swanson, J.F. Southern, and J.G. Fujimoto. "Assessing Atherosclerotic Plaque Morphology: Comparison of Optical Coherence Tomography and High Frequency Intravascular Ultrasound." *Brit. Heart J.* 77: 397-404 (1997).

Brezinski, M.E., G.J. Tearney, S.A. Boppart, E.A. Swanson, J.F. Southern, and J.G. Fujimoto. "Optical Biopsy with Optical Coherence Tomography, Feasibility for Surgical Diagnostics." *J. Surgical Res.* 71: 32-40 (1997).

Chinn, S.R., E.A. Swanson, and J.G. Fujimoto. "Optical Coherence Tomography using a Frequency-tunable Optical Source." *Opt. Lett.* 22: 340-42 (1997).

DiCarlo, C.D., W.P. Roach, D.A. Gagliano, S.A. Boppart, D.X. Hammer, A.B. Cox, and J.G. Fujimoto, "Comparison of Optical Coherence Tomography (OCT) Imaging of Cataracts with Histopathlogy." Submitted to *Investigat. Ophthalmol. Visual Sci.*

Fujimoto, J.G., S.A. Boppart, G.J. Tearney, B.E. Bouma, C. Pitris, and M.E. Brezinski. "High Resolution *In Vivo* Intraarterial Imaging with Optical Coherence Tomography." Submitted to *Circulat.*

Herrmann, J.M., M.E. Brezinski, B.E. Bouma, S.A. Boppart, C. Pitris, and J.G. Fujimoto. "Two and Three Dimensional High Resolution Imaging of the Human Oviduct with Optical Coherence Tomography." *Fertil. Steril.* Forthcoming.

Herrmann, J.M., C. Pitris, B.E. Bouma, S.A. Boppart, J.G. Fujimoto, and M.E. Brezinski. "High Resolution Imaging of Normal and Wsteoartheritic Cartilage with Optical Coherence Tomography." Submitted to *J. Rheumatol.*

Narayan, D.G., C.A. Toth, S. Boppart, M.R. Hee, J.G. Fujimoto, R. Birngruber, C.P. Cain, C.D. DiCarlo, and W.P. Roach. "A Comparison of Retinal Morphology Viewed by Optical Coherence Tomography and Light Microscopy." *Investigat. Ophthalmol. Visual Sci.* Forthcoming.

Tearney, G.J., M.E. Brezinski, J.F. Southern, B.E. Bouma, S.A. Boppart, and J.G. Fujimoto. "Optical Biopsy in Human Urologic Tissue using Optical Coherence Tomography." *J. Urol.* 157: 1915-19 (1997).

Tearney, G.J., M.E. Brezinski, B.E. Bouma, S.A. Boppart, C. Pitris, J.F. Southern, and J.G. Fujimoto. "*In Vivo* Endoscopic Optical Biopsy with Optical Coherence Tomography." *Sci.* 276: 2037-39 (1997).

Tearney, G.J., M.E. Brezinski, J.F. Southern, B.E. Bouma, S.A. Boppart, and J.G. Fujimoto. "Optical Biopsy in Human Gastrointestinal Tissue using Optical Coherence Tomography." *Am. J. Gastroenterol.* 92: 1800-04 (1997).

Tearney, G.J., B.E. Bouma, and J.G. Fujimoto. "High-speed Phase- and Group-delay Scanning with a Grating-based Phase Control Delay Line." *Opt. Lett.* 22: 1811-13 (1997).

Tong, Y.P. , P.M. W. French, J.R. Taylor, and J.G. Fujimoto. "All-solid-state Femtosecond Sources in the Near Infrared." *Opt. Commun.* 136: 235-38 (1997).

Toth, C.A., R. Birngruber, S.A. Boppart, M.R. Hee, J.G. Fujimoto, C.D. DiCarlo, E.A. Swanson, C.P. Cain, D. Narayan, G.D. Noojin, and W.P. Roach. "Argon Retinal Laser Lesions Evaluated *In Vivo* by Optical Coherence Tomography." *Am. J. Ophthalmol.* 123: 188-98 (1997).

Zuclich, J.A., S.T. Schuschereba, H. Zwick, S.A. Boppart, J.G. Fujimoto, F.E. Cheney, and B.E. Stuck. "A Comparison of Laser-induced Retinal

Damage from Infrared Wavelengths to that from Visible Wavelengths." *Lasers Light Ophthalmol.* 8: 15-29 (1997).

Conference Presentations

Boppart, B.A., J.M. Herrmann, C. Pitris, B.E. Bouma, G.J. Tearney, M.E. Brezinski, and J.G. Fujimoto. "Interventional Optical Coherence Tomography for Surgical Guidance." Submitted for presentation at the Conference on Lasers and Electro Optics, CLEO98, San Francisco, California, May 1998.

Boppart, S.A., M.E. Brezinski, B.E. Bouma, C. Pitris, J.F. Southern and J.G. Fujimoto. "Microsurgical Guidance using Optical Coherence Tomography." Conference on Lasers and Electro Optics CLEO'97, Baltimore, Maryland, May 18-23, 1997, paper CWD2.

Boppart, S.A., B.E. Bouma, C. Pitris, J.F. Southern, M.E. Brezinski, and J.G. Fujimoto. "Optical Coherence Tomographic Imaging of *In Vivo* Cellular Dynamics." Paper presented at the Advances in Optical Imaging and Photon Migration Conference, Orlando, Florida, March 9-13, 1998.

Bouma, B.E., G.J. Tearney, S.A. Boppart, B. Golubovic, I.P. Bilinsky, and J.G. Fujimoto. "Mode Locked Solid State Laser Sources for Optical Tomography." Coherence Domain Optical Methods in Biomedical Science and Clinical Applications, BIOS 97 International Biomedical Optics Symposium, SPIE, February 8-14, 1997, San Jose, California.

Brezinski, M.E., G.J. Tearney, S.A. Boppart, B.E. Bouma, N.J. Weissman, C. Pitris, J.G. Fujimoto. "Micron Scale Catheter Based *In Vivo* and *In Vitro* Imaging with Optical Coherence Tomography." Oral presentation, Transcatheter Cardiovascular Therapeutics, Washington, D.C., September 24-28, 1997.

Brezinski, M.E., J.M. Herrmann, C. Pitris, B.E. Bouma, S.A. Boppart, J.F. Southern, J.G. Fujimoto. "Ultrahigh Resolution Imaging of Normal and Osteoarthritic Cartilage Microstructure." Poster presentation, American College of Rheumatology National Scientific Meeting, Washington, D.C., November 8-12, 1997.

Brezinski, M.E., G.J. Tearney, S.A. Boppart, B. Bouma, E.A. Swanson, J.F. Southern, and J.G. Fujimoto. "*In Vivo* Imaging with Optical Coherence Tomography." American College of Cardiology 46th Annual Scientific Session, Anaheim, California, March 16-19, 1997

Brezinski, M.E., B.E. Bouma, S.A. Boppart, C. Pitris, J.F. Southern, and J.G. Fujimoto. "*In Vivo* High Resolution Imaging of Gastrointestinal Tissue using Optical Coherence Tomography." Paper presented at the Annual Meeting of the American Society for Gastrointestinal Endoscopy at Digestive Disease Week, Washington, D.C., May 11-14, 1997.

Brezinski, M.E., C. Pitris, S.A. Boppart, G.J. Tearney, J.F. Southern, and J.G. Fujimoto. "Micron Scale Optical Biopsy with Optical Coherence Tomography." Submitted for presentation to ASCO Annual Meeting, Denver, Colorado, May 17-20, 1997.

Chernikov, S.V., J.R. Taylor, V.P. Gapontsev, B.E. Bouma, and J.G. Fujimoto. "A 75-nm, 30-mW Superfluorescent Ytterbium Fiber Source Operating Around 10.6 mm." Conference on Lasers and Electro Optics CLEO '97, Baltimore, Maryland, May 18-23, 1997, paper CTuG8.

Coker, J.G. M.R. Hee, C.A. Puliafito, J.C. Szwartz, J.S. Duker, E. Reichel, J. S. Schuman, E.A. Swanson, and J.G. Fujimoto. "Prognosis and Anatomic Outcome of Macular Hole Surgery Assessed by Optical Coherence Tomography." Association for Research in Vision and Ophthalmology Annual Meeting, Fort Lauderdale, Florida, May 11-16, 1997, paper 3455-B56.

Fujimoto, J.G., G. Tearney, S. Boppart, C. Pitris, B. Bouma, J. Southern, and M. Brezinski. "New Techniques for High Resolution and High Speed Optical Coherence Tomography." New York Academy of Sciences and the Center for Advanced Technology at CUNY on Advances in Optical Biopsy and Optical Mammography, April 24-25, 1997, New York.

Fujimoto, J.G., B.E. Bouma, G.J. Tearney, S.A. Boppart, C. Pitris, J.F. Southern, and M.E. Brezinski. "High Speed and High Resolution Optical Coherence Tomography using Femtosecond Lasers." Conference on Lasers and Electro Optics CLEO'97, May 18-23, 1997, Baltimore, Maryland, (invited) paper CTuS1.

Fujimoto, J.G., G.J. Tearney, S.A. Boppart, C. Pitris, and B.E. Bouma. "High Speed High Resolution Optical Coherence Tomography for Optical Biopsy." LASERmed 97, 13th International Congress Laser Medicine, Munich, Germany, June 18-20, 1997.

Fujimoto, J.G., G.J. Tearney, S.A. Boppart, C. Pitris, B.E. Bouma, J. Herrmann, J.F. Southern, and M.E. Brezinski. "Optical Coherence Tomographic in Medicine." Fifth Congress of the International

Society for Skin Imaging, Vienna, Austria, September 25-27, 1997, invited talk.

Fujimoto, J.G. "Optical Coherence Tomography for Biomedical Imaging." The International Topical Workshop on Contemporary Photonic Technologies, Tokyo, Japan, January 11-15, 1998, invited talk.

Herrmann, J.M., C. Pitris, B.E. Bouma, S.A. Boppart, J.G. Fujimoto, and M.E. Brezinski. "Two and Three Dimensional Imaging of Normal and Osteoarthritic Cartilage Microstructure with Optical Coherence Tomography." Paper presented at the Advances in Optical Imaging and Photon Migration Conference, Orlando, Florida, March 9-13, 1998.

Herrmann, J.M., S.A. Boppart, B.E. Bouma, G.J. Tearney, C. Pitris, M.E. Brezinski, and J.G. Fujimoto. "Real Time Imaging of Laser Intervention with Optical Coherence Tomography." Paper presented at the Advances in Optical Imaging and Photon Migration Conference, Orlando, Florida, March 9-13, 1998.

Huang, L.N., J.S. Schuman, T.P. Kloizman, L. Pieroth, N. Wang, M.R. Hee, J.G. Coker, C.A. Puliafito, J.G. Fujimoto, and E.A. Swanson. "The Comparison of Nerve Fiber Layer Thickness in Glaucomatous Monkey Eyes Measured by Optical Coherence Tomography." Association for Research in Vision and Ophthalmology Annual Meeting, Fort Lauderdale, Florida, May 11-16, 1997, paper 3913-B514.

Kim, V.Y., S. Roh, L. Pieroth, T. Pedut-Kloizman, M. Hee, J.G. Coker, J.C. Szwartz, C.A. Puliafito, J.S. Schuman, E.A. Swanson, J.G. Fujimoto, and J.S. Duker. "Quantification of Nerve Fiber Layer and Retinal Thickness using Optical Coherence Tomography in Patients with Human Immunodeficiency Virus Infection." Association for Research in Vision and Ophthalmology Annual Meeting, Fort Lauderdale, Florida, May 11-16, 1997, paper 5151-B658.

Pieroth, L., J.S. Schuman, E. Hertzmark, M.R. Hee, J.G.Coker, P.Y. Chung, T. Pedut-Kloizman, C.A. Puliafito, C. Mattox, J.G. Fujimoto, and E.A. Swanson. "Comparison of the Nerve Fiber Layer by Optical Coherence Tomography Before and After Intraocular Pressure Lowering Procedures." Association for Research in Vision and Ophthalmology Annual Meeting, Fort Lauderdale, Florida, May 11-16, 1997, paper 3916-B517.

Pitris, C., S.A. Boppart, B.E. Bouma, G. Tearney, J.G. Fujimoto, and M.E. Brezinski. "High Resolution In-vivo Intravascular Imaging with Optical Coherence Tomography." Paper presented at the Advances in Optical Imaging and Photon Migration Conference, Orlando, Florida, March 9-13, 1998.

Tearney, G.J., S.A. Boppart, B.E. Bouma, C. Pitris, M.E. Brezinski, J.F. Southern, E. A. Swanson, and J.G. Fujimoto. "High Speed Catheter/Endoscopic Optical Coherence Tomography for the Optical Biopsy of *in vivo* Tissues." Conference on Lasers and Electro Optics CLEO '97, Baltimore, Maryland, May 18-23, 1997, paper CWD5.

Pitris, C., S.A. Boppart, B.E. Bouma, and J.G. Fujimoto. "Cellular and Neoplastic Tissue Imaging with Optical Coherence Tomography." Submitted for presentation at the Conference on Lasers and Electro Optics, CLEO98, San Francisco, California, May 1998.

Tearney, G.J., M.E. Brezinski, B.E. Bouma, J.F. Southern, and J.G. Fujimoto. "High Resolution Imaging of Urologic Tissues using Optical Coherence Tomography." American Urological Association 1997 Annual Meeting, New Orleans, Louisiana, April 12-17, 1997, Abstract 479.

Tearney, G.J., B.E. Bouma, S.A. Boppart, M.E. Brezinski, J.F. Southern, E.A. Swanson, and J.G. Fujimoto. "Endoscopic Optical Coherence Tomography." Tomography and Spectroscopy of Tissue, BIOS 97 International Biomedical Optics Symposium, SPIE, San Jose, California, February 8-14, 1997,

Toth, C.A., D.G. Narayan, W.P. Roach, S.A. Boppart, M.R. Hee, C.D. DiCarlo, E.A. Swanson, C.P. Cain, G.D. Noojin, and J.G. Fujimoto. "Retinal Injury Evaluated using Optical Coherence Tomography." BIOS 97 International Biomedical Optics Symposium, SPIE, San Jose, California, February 8-14, 1997.

Toth, C.A., D.G. Narayan, W.P. Roach, S.A. Boppart, M.R. Hee, J.G. Fujimoto, R. Birngruber, C.D. DiCarlo, C.P. Cain, and G.D. Noojin. "Analyzing Retinal Laser Effects: Old and New Techniques." Conference on Lasers and Electro Optics CLEO '97, Baltimore, Maryland, May 18-23, 1997, (invited) paper CTuT1.

1.16 Analytical Confirmation of Stochastic Soliton Formulation

Project Staff

John M. Fini, Professor Peter L. Hagelstein and Professor Hermann A. Haus

Optical solitons have been demonstrated in regimes useful for long-distance communications and the generation of squeezed light. Quantum effects are of fundamental importance in such systems, since the dominant noise is often of quantum-mechanical origin. Previous work[102] has led to a good theoretical understanding of soliton propagation and interactions, in agreement with experiment.[103]

An alternative stochastic formulation of the same quantum evolution was given by Drummond and Carter early on,[104] and has been used numerically to evaluate squeezing. Until now, no direct comparison has been made of results of the two formulations.

We have applied the stochastic theory to the computation of basic, interesting quantities—the spreading of position and phase in a freely propagating soliton[105] (see Figure 20). The result is that the linearized stochastic theory agrees exactly with predictions of the operator theory.[106] This validates the stochastic method and allows greater confidence in its further application.

Figure 20. This figure depicts accumulated quantum uncertainty in the position of pulses in a communications system. The accumulating uncertainty in position, and thus in arrival time, of a pulse places fundamental limitations on the communication rate.

In the second-quantized formulation, $\hat{\phi}(x,t)$ is the operator analog of the field amplitude and evolves according to

$$\frac{\partial}{\partial t}\hat{\phi} = i\left[-\frac{1}{2} + \frac{1}{2}\frac{\partial^2}{\partial x^2} + c\hat{\phi}^{+}\hat{\phi}\right]\hat{\phi} \quad (1)$$

The basic equations of motion for the stochastic formalism govern the formal, complex variables ϕ and ϕ^{+}. The evolution,

$$\frac{\partial \phi}{\partial t} = i\left[-\frac{1}{2} + \frac{1}{2}\frac{\partial^2}{\partial x^2} + c\phi^{+}\phi\right]\phi + (ic)^{1/2}\phi\xi(x,t) \quad (2)$$

$$\frac{\partial}{\partial t}\phi^{+} = -i\left[-\frac{1}{2} + \frac{1}{2}\frac{\partial^2}{\partial x^2} + c\phi^{+}\phi\right]\phi^{+} + (-ic)^{1/2}\phi^{+}\xi^{+}(x,t) \quad (3)$$

is, according to its derivation, exactly equivalent to the operator equation.

Traditional soliton perturbation theory extracts solvable modes of the linearized equations of motion. Adapting this basic principle to the stochastic differential equations (2) and (3), we can similarly project out four special modes which are decoupled from all other modes of the system. Having solved the SDEs for these modes, we can then relate them to physical variables of interest in accordance with the stochastic construction.

Specifically, just as perturbation theory applied to equation (1) gives the evolution of position and momentum operators,

$$\frac{\partial}{\partial t}\Delta\hat{x} = \Delta\hat{p} \quad (4)$$

so do the stochastic equations give,

$$\frac{\partial}{\partial t}c_{x,\,\mathrm{stoch}} = c_{p,\,\mathrm{stoch}} + \mathrm{noise} \quad (5)$$

102 J.P. Gordon and H.A. Haus, *Opt. Lett.* 11: 665 (1986); Y. Lai and H.A. Haus, *Phys. Rev. A* 40: 844 (1989); Y. Lai and H.A. Haus, *Phys. Rev. A* 40: 854 (1989); P.L. Hagelstein, *Phys. Rev. A* 54: 2426 (1996).

103 H.A. Haus and W.S. Wong, *Rev. Mod. Phys.* 68: 423 (1996).

104 P.D. Drummond and S.J. Carter, *J. Opt. Soc. Am. B* 4: 1565 (1987).

105 J.M. Fini, P.L. Hagelstein, and H.A. Haus, *Phys. Rev. A*, forthcoming.

106 H.A. Haus and Y. Lai, *J. Opt. Soc. Am. B* 7: 386 (1990); Y. Lai, *J. Opt. Soc. Am. B* 10: 475 (1993); P.L. Hagelstein, *Phys. Rev. A* 54: 2426 (1996).

Equation (5) and the corresponding evolutions for n, p, and θ constitute a linear system, easily solved in terms of the complex noise drives. The variables $c_{x,stoch}$, etc., represent the statistics of the quantum operators $\hat{x}$, $\hat{p}$, etc., but only indirectly. To connect quantum and stochastic statistics, we must carefully follow the (somewhat counter-intuitive) rules prescribed by the Drummond and Carter construction.[107]

The basic statistical correspondence behind the stochastic method looks deceptively simple:

$$\langle (\hat{\phi}^{\dagger})^m \hat{\phi}^n \rangle = \langle (\phi^+)^m \phi^n \rangle \qquad (6)$$

We must be cautious because while $\hat{\phi}$ and $\hat{\phi}^{\dagger}$ are operators and are Hermitian conjugate to one another, ϕ and ϕ^+ are complex numbers and are generally *not* conjugate. Care must be taken with the ordering of operators. The functions ϕ and ϕ^+ must not be thought of as physical variables, except insofar as they generate physical moments through equation (6). Practically, this means that the stochastic method involves traditional operator algebra as well as stochastic manipulations.

In calculating variances of the soliton position and phase, the correct correspondences have the form,

$$\langle \Delta \hat{x}^2 \rangle = \langle c^2_{x,\,stoch} \rangle + \text{constant commutator} \qquad (7)$$

The stochastic moment, computed by solving the system (2) and (3) is then combined with the commutator term resulting from operator algebra. Commutators give us the initial vacuum fluctuations of a coherent state, while stochastic moments add subsequent deviations from coherent-state statistics in quadrature. The result is in full agreement with previous results on the evolution of spreading in soliton position, phase, momentum, and photon number.

The calculation we have done allows us to place greater confidence in the stochastic method, whether it is applied analytically or numerically. It serves as a model calculation, bringing out several nonintuitive aspects of the theory. Finally, we have found that all essential features of this calculation and the stochastic method can be captured in a simplified single-nonlinear-oscillator tutorial.

1.16.1 Publication

Fini, J.M., P.L. Hagelstein, and H.A. Haus. "Agreement of Stochastic Soliton Formalism with Second-Quantized and Configuration-Space Models." *Phys. Rev. A*. Forthcoming.

1.17 Long-Time Evolution of Soliton Position and Phase in the Second-Quantized Model

Project Staff

John M. Fini, Professor Peter L. Hagelstein, and Professor Hermann A. Haus

Quantum models of soliton propagation have been used to understand noise and interaction of these pulses in optical fiber. Recently, Hagelstein[108] has demonstrated a simple and effective approach to quantum optics problems; using a photon configuration-space model based on the familiar second-quantized theory,[109] he has computed the long-time evolution (beyond the linearization) of soliton position and phase spread.

While the use of this approach may have far-reaching implications for the more general use of photon configuration space, the calculation itself does not involve any radical new assumptions. To demonstrate this, we show that free-particle dynamics for soliton position and phase are the result of the Hartree approximation and of large photon number.[110] By rederiving these dynamics, we clarify the essential features of the system and demonstrate that the calculation can be made entirely within the second-quantized framework. In particular, the issue of defining a quantum phase operator for solitons is explored.

Soliton position and phase follow free particle dynamics. That is, they act as coordinates evolving with no applied force. The intuitive picture corresponding to this motion is essentially classical (Fig-

107 P.D. Drummond and S.J. Carter, *J. Opt. Soc. Am. B* 4: 1565 (1987); C.W. Gardiner, *Handbook of Stochastic Methods for Physics, Chemistry, and the Natural Sciences* (New York: Springer-Verlag, 1985).

108 P.L. Hagelstein, *Phys. Rev. A* 54: 2426 (1996).

109 Y. Lai and H.A. Haus, *Phys. Rev. A* 40: 844 (1989); Y. Lai and H.A. Haus, *Phys. Rev. A* 40: 854 (1989).

110 J.M. Fini, P.L. Hagelstein, and H.A. Haus, "Nonperturbative Calculation of Sloiton Variables." Submitted to *Phys. Rev. A.*

ure 21). These dynamics are reflected in the appearance of conserved, conjugate variables (number and momentum) in the linearized operator theory[111] and are clearly spelled out in the configuration space calculation.

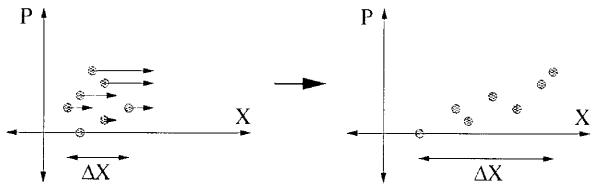

Figure 21. The evolution in phase space of a collection of free particles is illustrated. Spreading in position results from either quantum-mechanical or statistical mechanical evolution.

The case of position is simpler. Here we have the exact relation:

$$[\hat{X},\hat{H}] = i\hbar\hat{P}/M \tag{8}$$

$$[\hat{P},\hat{H}] = 0 \tag{9}$$

Hagelstein shows this by separating center-position and relative position parts of the Hamiltonian. However, we have obtained these relations explicitly by manipulating photon operators, consistent with the definitions of Lai and Haus.[112] From here, Hagelstein's time-dependence of position spread is simply obtained from the standard rules for evolving quantum expectations (in any picture):

$$\left\langle \Delta\hat{X}^2 \right\rangle = \left\langle \Delta\hat{P}^2 \right\rangle_o t^2/M^2 + \left\langle \Delta\hat{X}\Delta\hat{P} + \Delta\hat{P}\Delta\hat{X} \right\rangle_o t/M + \left\langle \Delta\hat{X}^2 \right\rangle_o \tag{10}$$

The case of phase spreading is not as simple. It is not even clear that we can write down a valid phase operator in terms of photon operators. The problem of finding a valid phase operator for a single oscillator has been studied for many years.[113] Satisfactory results are possible in the limit of high photon number. An optical field is not a single oscillator, but rather many operators. For solitons, we want to identify a single phase for this multimode field. This suggests a favored mode, or a special annihilation operator $\hat{A}$ associated with the central-phase. With infinitely many $\hat{\phi}(x)$ s, it is not obvious *a priori* that any special combination exists.

Using the Hartree approximation in the limit of large photon number allows us to overcome these difficulties. On the one hand, a Hartree product state corresponding to a soliton has a well-defined "mode" that all of the photons are in, allowing us to associate a single $\hat{A}$ with the soliton. It then makes sense to think of N and θ as (approximately) conjugate variables,

$$[\hat{\theta},\hat{N}] = i \tag{11}$$

On the other hand, there is a well-defined energy associated with the number of a Hartree product state, so that we can write the effective Hamiltonian seen by $\hat{\theta}$,

$$\hat{H}_\theta = \hbar\omega\left(\hat{N}\right). \tag{12}$$

While the issues relating to these two physical statements are complicated, we assert that they present a correct and intuitive description for how soliton phase should work.[114] We will now show that they are all that is needed to obtain free-particle dynamics fully analogous to equations (8) and (9).

From the above assumptions, we obtain quite directly

$$[\hat{\theta},\hat{H}] = i\hbar\frac{d\omega}{dN} \tag{13}$$

$$[\hat{N},\hat{H}] = 0. \tag{14}$$

Equation (13) in essence identifies a "velocity" operator associated with $\hat{\theta}$, which is a function of N. The second states that N, and thus also the "velocity," is stationary. The two represent free-particle dynamics in exactly the same way that equations (8) and (9) do.

Finding the time-dependence of phase spread is again only a matter of applying standard quantum methods. The result, in the limit relevant to the soliton problem is

111 H.A. Haus and Y. Lai, *J. Opt. Soc. Am. B* 7: 386 (1990); Y. Lai, *J. Opt. Soc. Am. B* 10: 475 (1993).

112 Y. Lai and H.A. Haus, *Phys. Rev. A* 40: 844 (1989).

113 M.M. Nieto, *Physica Scripta* T48: 5 (1993).

114 P.L. Hagelstein, *Phys. Rev. A* 54: 2426 (1996).

$$\langle \Delta\theta^2 \rangle = \langle \theta^2 \rangle_0 + [\omega''(n_0)]^2 \langle \Delta n^2 \rangle_0 t^2 , \quad (15)$$

where $\omega''(n_0) = \left(\frac{d^2\omega}{dN^2} \right)_{n_0}$. This has previously been shown to agree with the linearized theory of Haus and Lai.

By continuing the arguments of Hagelstein, we have arrived at what is essential to the free-particle dynamics of soliton position and phase. We have demonstrated that these dynamics can be derived entirely within the second-quantized formulation and have identified the characteristics of solitons which allow us to find a quantum phase operator. We now have an obvious approach to identifying phase for more general fields.

1.17.1 Publication

Fini, J.M., P.L. Hagelstein, and H.A. Haus. "Nonperturbative Calculation of Soliton Variables." Submitted to *Phys. Rev. A*.

1.18 Local Consequences of Strong Phonon Excitation in a Lattice

Project Staff

Professor Peter L. Hagelstein

1.18.1 Hybrid Lattice Description

We are familiar with two descriptions of the motion of atoms in a lattice. We can describe the position of the atom in terms of the center of mass location of the nucleus. This would be appropriate for describing energetic two-body interactions, such as the dislodging of an atom in a lattice by an MeV neutron. Alternatively, we can describe the local atomic dynamics in terms of the vibrational modes of the lattice. Such a description would be useful in analyzing the response of an atom and its surroundings in the case of low energy transfer, as might occur in the case of Bragg scattering of a neutron from a crystal. These two different descriptions are ultimately completely equivalent, as described through the quantum relation

$$\hat{\mathbf{R}}_i = \mathbf{R}_i^0 + \sum_m \mathbf{u}_i(m)\hat{q}_m . \quad (16)$$

The position operator of the ith atom is $\hat{\mathbf{R}}_i$, and the amplitude of the mth phonon mode is $\hat{q}_m$. The success of this point of view is so complete that by now we think only in terms of one view or the other, all the while recognizing that the two approaches are completely equivalent.

But what happens when the lattice is forced to exhibit interesting behavior both on the local level and globally as well? Suppose we set up a problem in which a delocalized phonon mode is very highly excited, which necessitates a phonon point of view, and then ask questions about the detailed local dynamics such as the atom-atom correlation, which necessitates a local position point of view. While the phonon point of view allows for a convenient description of the global dynamics, it is not convenient at all for treating that atom-atom interaction on a small scale. Conversely, while a position operator description is very good at describing the local atom-atom correlations, the corresponding description of the global excitation becomes highly inconvenient.

This discussion motivates the introduction of a novel hybrid description, in which the global excitation is described through the use of a single phonon amplitude, and in which the local dynamics are described in terms of a residual position operator. We propose the hybrid construction[115]

$$\hat{\mathbf{R}}_i = \bar{\hat{\mathbf{R}}}_i + \mathbf{u}_i\hat{q} . \quad (17)$$

The residual local position operator is $\bar{\hat{\mathbf{R}}}_i$, which is made up of the contributions of all the other phonon modes and which behaves very much like a local position operator. In the absence of large excitation in the phonon mode that is singled out, results obtained with the residual operator would be indistinguishable from results obtained using the true position operator when the lattice is large. A schematic of this construction is given in Figure 22.

115 P.L. Hagelstein, "Atom-atom Correlation in the Presence of Strong Terahertz Phonon Excitation," *Phil. Mag. B*, forthcoming.

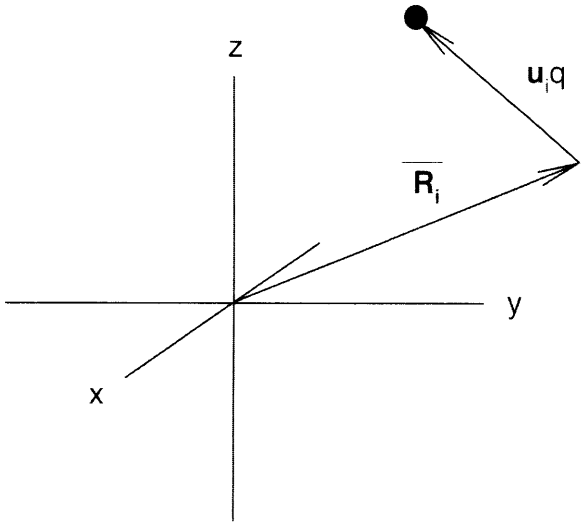

Figure 22. Schematic of contributions of the highly excited phonon mode and residual position operator to the atomic position in a lattice.

1.18.2 Quantum Mechanical Versus Classical View

If a phonon mode is highly excited, we usually picture the resulting dynamics in our mind's eye in terms of a classical picture. We see atoms as masses and the interaction with other atoms in terms of springs (very small springs, but springs nonetheless). The motion on the atomic scale is that of an atom vibrating synchronously with other atoms, oscillating at a characteristic frequency that may be on the order of a few terahertz in the example that interests us here. In our classical picture, the more highly excited the lattice is, the larger the local amplitude of vibrations. If the total vibrational energy of the lattice is E_L, then we imagine that each individual atom has an energy that is on the order of

$$E_a \sim \frac{E_L}{N}, \tag{18}$$

where N is the number of atoms in the lattice. For example, if the average local atomic energy is E_a = 5 meV, and if there are N = 10^{10} atoms present (we imagine here a small lattice), then the total lattice energy E_L is 50 MeV—a very large total energy for the many-atom lattice.

The quantum description of the lattice is not very different in most respects from the classical description. Ehrenfest's theorem ensures that the dynamics of the average position operator matches that of the classical positions for all local potential terms up to second order. This means that for all low-order interactions with atoms in the lattice that our classical intuition is basically sound. For example, in a gentle collision of a neutron with an atom in the lattice, the classical picture will give the correct answer on average for energy transfer. This is not to say that on closer inspection there are not quantum effects that show up, for surely there are. Instead, we have an assurance that on average each atom responds as if it had an energy on average on the order of E_L/N. It is never the case that the total lattice energy somehow shows up at one atomic site in such low-order interactions.

Within the quantum description outlined above, the excitation of the lattice with the total lattice energy E_L appears explicitly in the description of the atomic position. For example, in writing

$$\hat{\mathbf{R}}_i = \overline{\hat{\mathbf{R}}_i} + \mathbf{u}_i \hat{q} \tag{19}$$

we observe that the phonon coordinate $\hat{q}$ is part of a many-particle quantum system with a total energy that can be 50 MeV in our example. Each atom, in fact, does know about the total lattice energy of the excited mode; whether any observable effects ever arise is another story altogether. Certainly it can be shown that no significant energy exchange from the highly excited mode can occur through first order interactions that are low order in $\hat{q}$. But whether there exist first order interactions that are very high order in $\hat{q}$ or second order interactions that behave differently must be determined by direct computation or by experiment. This is presently an open question, one that has only just been posed in our work.

1.18.3 Impact of Strong Phonon Excitation on Local Correlations

Any interaction that might exhibit interesting new effects in which a larger fraction of the total lattice energy will be involved must be highly nonlinear in $\hat{q}$. Consequently, we seek any very strong interactions that are highly nonlinear in the atomic positions as candidates that may show new physics. One obvious candidate is the Coulomb interaction at short range between the atomic nuclei of neighboring atoms. When two atoms approach to within 50 fermis of one another, the associated Coulomb interaction is very strong (the associated potential energy is about 300 keV for protons), and the interaction is exceedingly nonlinear in $\hat{q}$. Of course, it is a rare occurrence that

two atoms will ever be so close, but when they are we might expect that the resulting dynamics may be sensitive to the total lattice energy in some way.

To investigate this, we work with a hybrid version of the relative atom-atom displacement operator

$$\Delta\hat{\mathbf{R}}_{ij} = \overline{\Delta\hat{\mathbf{R}}}_{ij} + \Delta\mathbf{u}_{ij}\hat{q}, \tag{20}$$

where $\overline{\Delta\hat{\mathbf{R}}}_{ij}$ is the residual atom-atom displacement in the absence of the highly excited mode. Any new effects will show up in modifications of the lattice wavefunction, which we might approximate with the hybrid description in terms of

$$\Psi \rightarrow \Psi(\overline{\mathbf{R}}_i, \overline{\mathbf{R}}_j, q). \tag{21}$$

The total lattice wavefunction Ψ on the left knows in detail about the dynamics of all the atoms in the lattice; the hybrid version $\Psi(\overline{\mathbf{R}}_i, \overline{\mathbf{R}}_j, q)$ focuses our attention on the highly excited mode and on the local residual dynamics of the two atoms. The relevant Schrödinger equation is then of the form

$$\left[-\frac{\hbar^2\nabla^2}{2M_i} - \frac{\hbar^2\nabla^2}{2M_j} - \frac{\hbar^2}{2M_q}\frac{\partial^2}{\partial q^2} + \frac{1}{2}M_q\omega_q^2 q^2 + V(\overline{\mathbf{R}}_i, \overline{\mathbf{R}}_{j,q})\right]\Psi = E\Psi. \tag{22}$$

Approximate solutions of this equation can be developed according to

$$\Psi = \phi(q)\psi(\overline{\mathbf{R}}_i, \overline{\mathbf{R}}_j, q), \tag{23}$$

in the general spirit of the Born-Oppenheimer approximation. This approach is presently under investigation.

1.18.4 Possibility of Lattice-Induced Recoil

We are interested in the possibility that some of the energy in the highly excited phonon mode may be transferred to the local degrees of freedom. We are imagining that the lattice is highly excited so that energy is readily available, and we are interested in the high order nonlinearity of the Coulomb potential at close range which we hope will mediate the energy transfer. The computation of reaction rates for this process involving protons for example follows from Fermi's Golden Rule

$$\gamma = \frac{2\pi}{\hbar}\left|\left\langle \Psi_f \left| \frac{e^2}{|\mathbf{R}_i - \mathbf{R}_j|} \right| \Psi_i \right\rangle\right|^2 \rho(E_f). \tag{24}$$

If the phonon mode degree of freedom were separable from the local degrees of freedom

$$\Psi \approx \phi(q)\psi(\overline{\mathbf{R}}_i, \overline{\mathbf{R}}_j), \tag{25}$$

then the computation of the reaction rate is straightforward, and this model leads to significant rates of lattice-induced recoil. The inclusion of correlation between the local degrees of freedom and the phonon mode amplitude as discussed above complicates matters and results in a significant reduction of the predicted recoil emission rates from the separated result. We are pursuing this to try to obtain reliable estimates of the rate for this effect.

1.19 Steady-State Hydrodynamic Ablation

Project Staff

Professor Peter L. Hagelstein, Susan Sujono

In many x-ray laser experiments, an intense laser is incident on a solid surface in line focus, and hot plasma is ablated. We are interested in the temperature and density profile in order to understand whether the plasma so created is suitable for the development of gain in the EUV and soft x-ray regimes. While the plasma evolution is transient, it is of interest to understand the steady state limit of the ablation, most interestingly because it represents an upper limit of the capability of the plasma to conduct heat from the critical surface to the low-density region where gain is expected.

We have explored both one-dimensional and two dimensional versions of the problem.[116] The cylindrical expansion model in one dimension provides a very good approximation for the two-dimensional problem. For this case, we seek solutions of the coupled hydrodynamic equations

$$\frac{1}{r}\frac{d}{dr}(r\rho v) = 0 \tag{26}$$

$$v\frac{d}{dr}v = -\frac{1}{r}\frac{d}{dr}P \tag{27}$$

116 S. Sujono, *Analytical Study of Steady State Plasma Ablation from Soft X-ray Laser Target*, M.Eng. thesis, Department of Electrical Engineering and Computer Science, MIT, 1997.

$$v\frac{d}{dr}T = -\frac{2}{3}T\frac{1}{r}\frac{d}{dr}(rv) + \frac{2}{3}\frac{1}{N}\frac{1}{r}\frac{d}{dr}\left(r\kappa\frac{d}{dr}T\right). \quad (28)$$

Temperature and velocity profiles have been computed numerically. We have also investigated the use of analytic models, and we have found that accurate normalized velocity and temperature profiles can be developed from few parameter fits according to

$$u(\xi) = 1 + \alpha_3(1 - e^{-\alpha_1\xi^{\alpha_2}}) \quad (29)$$

$$\tau(\xi) = e^{-\beta_1\xi^{\beta_2}}. \quad (30)$$

Here u is the plasma velocity in terms of the sound speed at the critical surface, and τ is the temperature normalized to the critical surface value. The variable ξ is the logarithmic spatial coordinate $\ln(r/r_0)$ where r_0 is the radius associated with the critical surface. These results are illustrated in Figure 23.

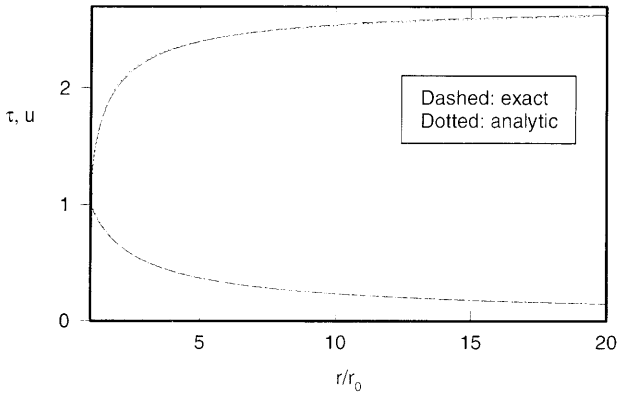

Figure 23. Numerical solution and analytic solutions for u and τ for steady state ablation in cylindrical geometry.

1.19.1 Thesis

Sujono, S. *Analytical Study of Steady State Plasma Ablation from Soft X-ray Laser Target.* M.Eng thesis, Department of Electrical Engineering and Computer Science, MIT, 1997.